Article

# Spectroscopic and Computational Studies of Co Corrinoids: Spectral and Electronic Properties of the Biologically Relevant Base-On and Base-Off Forms of Co Cobalamin

Troy A. Stich, Nicole R. Buan, and Thomas C. Brunold

*J. Am. Chem. Soc.*, **2004**, 126 (31), 9735-9749• DOI: 10.1021/ja0481631 • Publication Date (Web): 17 July 2004



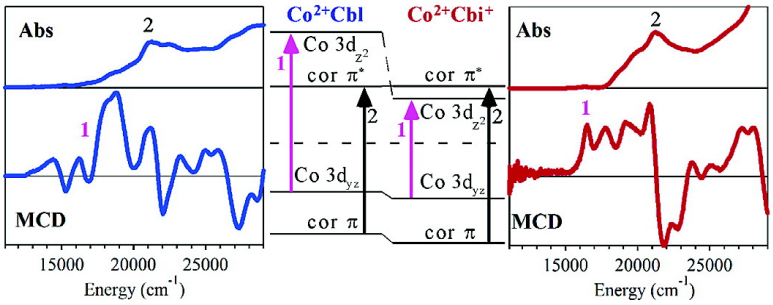


## More About This Article

Additional resources and features associated with this article are available within the HTML version:

- Supporting Information
- Links to the 6 articles that cite this article, as of the time of this article download
- Access to high resolution figures
- Links to articles and content related to this article
- Copyright permission to reproduce figures and/or text from this article

View the Full Text HTML

J|A|C|S
ARTICLES
Published on Web 07/17/2004

# Spectroscopic and Computational Studies of $Co^{2+}$Corrinoids: Spectral and Electronic Properties of the Biologically Relevant Base-On and Base-Off Forms of $Co^{2+}$Cobalamin

Troy A. Stich, Nicole R. Buan,† and Thomas C. Brunold*

*Contribution from the Department of Chemistry, University of Wisconsin-Madison, Madison, Wisconsin 53706*

Received March 30, 2004; E-mail: brunold@chem.wisc.edu

***Abstract:*** $Co^{2+}$cobalmain ($Co^{2+}$Cbl) is implicated in the catalytic cycles of all adenosylcobalamin (AdoCbl)-dependent enzymes, as in each case catalysis is initiated through homolytic cleavage of the cofactor's Co−C bond. The rate of Co−C bond homolysis, while slow for the free cofactor, is accelerated by 12 orders of magnitude when AdoCbl is bound to the protein active site, possibly through enzyme-mediated stabilization of the post-homolysis products. As an essential step toward the elucidation of the mechanism of enzymatic Co−C bond activation, we employed electronic absorption (Abs), magnetic circular dichroism (MCD), and resonance Raman spectroscopies to characterize the electronic excited states of $Co^{2+}$Cbl and $Co^{2+}$cobinamide ($Co^{2+}$Cbi$^+$, a cobalamin derivative that lacks the nucleotide loop and 5,6-dimethylbenzimazole (DMB) base and instead binds a water molecule in the lower axial position). Although relatively modest differences exist between the Abs spectra of these two $Co^{2+}$corrinoid species, MCD data reveal that substitution of the lower axial ligand gives rise to dramatic changes in the low-energy region where $Co^{2+}$-centered ligand field transitions are expected to occur. Our quantitative analysis of these spectral changes within the framework of time-dependent density functional theory (TD-DFT) calculations indicates that corrin-based $\pi \rightarrow \pi^*$ transitions, which dominate the $Co^{2+}$corrinoid Abs spectra, are essentially insulated from perturbations of the lower ligand environment. Contrastingly, the $Co^{2+}$-centered ligand field transitions, which are observed here for the first time using MCD spectroscopy, are extremely sensitive to alterations in the $Co^{2+}$ ligand environment and thus may serve as excellent reporters of enzyme-induced perturbations of the $Co^{2+}$ state. The power of this combined spectroscopic/computational methodology for studying $Co^{2+}$corrinoid/enzyme active site interactions is demonstrated by the dramatic changes in the MCD spectrum as $Co^{2+}$Cbi$^+$ binds to the adenosyltransferase CobA.

## 1. Introduction

Coenzyme $B_{12}$ (adenosylcobalamin, AdoCbl) has long been known to serve as an enzymatic cofactor for biological radical initiated rearrangement reactions.[1] This cofactor (Figure 1) consists of a low-spin $Co^{3+}$ ion equatorially ligated by the four nitrogens of a highly substituted macrocycle (the corrin ring) and coordinated in the "lower" axial position by the nitrogen of a pendant 5,6-dimethylbenzimidazole (DMB) base.[2] A 5′-deoxyadenosyl (Ado) group, bound to the metal center through its 5′-carbon, occupies the "upper" coordination site to complete a six-coordinate, distorted octahedral ligand environment of the $Co^{3+}$ center.[3] This organometallic bond is unique in nature, and although modestly strong in the isolated cofactor ($30 \pm 2$ kcal/mol bond dissociation enthalpy),[4] it lies at the heart of the reactivity when the cofactor is bound to $B_{12}$-dependent enzymes.

AdoCbl-dependent enzymes have been shown to lower the Co−C bond dissociation enthalpy by as much as 17 kcal/mol,[5] increasing the rate constant for bond homolysis by 12 orders of magnitude.[5−7] Co−C bond homolysis results in the formation of a five-coordinate $Co^{2+}$cobalamin ($Co^{2+}$Cbl) and an Ado$^\bullet$ radical that abstracts a hydrogen atom from the substrate molecule as the first step in the protein-mediated rearrangement reaction.[8] Two general schemes can be envisioned to rationalize the tremendous rate enhancement for the formation of the $Co^{2+}$Cbl/Ado$^\bullet$ radical pair accomplished by $B_{12}$-dependent enzymes. The first invokes a mechanism whereby the protein destabilizes the AdoCbl "ground" state, for example, through protein-induced folding of the corrin macrocycle, which could lead to steric crowding of the upper axial ligand, and/or modulation of the lower axial Co−N bond properties. However, our recent spectroscopic and computational studies on free and enzyme-bound AdoCbl afforded considerable evidence against $Co^{3+}$Cbl destabilization as contributing significantly to the

† Present address: Department of Bacteriology, University of Wisconsin-Madison, Madison, WI 53706.

(1) Banerjee, R., Ed. *Chemistry and Biochemistry of $B_{12}$*; Wiley-Interscience: New York, 1999.
(2) Hodgkin, D. C. P. J.; Robertson, J. H.; Trueblood, K. N.; Prosen, R. J.; White, J. G. *Nature* **1956**, *176*, 325−328.
(3) Lenhert, P. G.; Hodgkin, D. C. *Nature* **1961**, *192*, 937−938.
(4) Hay, B. P.; Finke, R. G. *J. Am. Chem. Soc.* **1986**, *108*, 4820−4829.
(5) Chowdhury, S.; Banerjee, R. *Biochemistry* **2000**, *39*, 7998−8006.
(6) Brown, K. L.; Zou, X. *J. Inorg. Biochem.* **1999**, *77*, 185−195.
(7) Marsh, E. N. G.; Ballou, D. P. *Biochemistry* **1998**, *37*, 11864−11872.
(8) Banerjee, R. *Biochemistry* **2001**, *40*, 6191−6198.

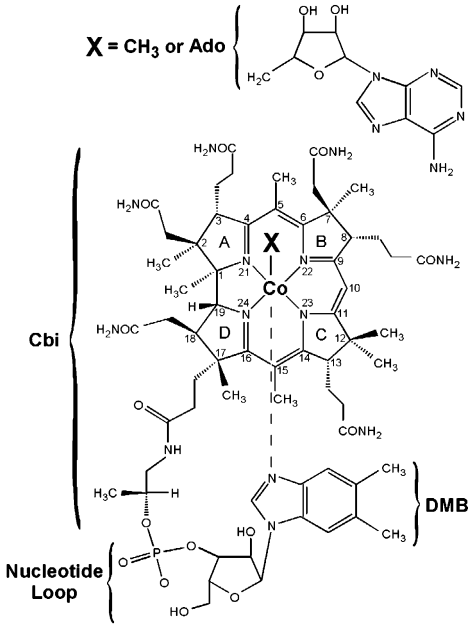


***Figure 1.*** Chemical bonding and numbering scheme for the biologically active forms of cobalamin, where X indicates the upper axial ligand.

Co−C bond activation.[9,10] The other scheme invokes stabilization of the Ado• and $Co^{2+}$Cbl post-homolysis products. The protein could achieve such stabilization through tight binding of the Ado• moiety and/or tuning of the geometric and electronic properties of the $Co^{2+}$Cbl species, for example, by repositioning of the lower axial ligand or modulation of the corrin ring conformation. In this regard, it is interesting to note that two classes of $B_{12}$-dependent enzymes have evolved that differ with respect to the mode of cofactor coordination in the enzyme active site. The "base-on" family (e.g., diol dehydratase)[11] binds intact AdoCbl, maintaining the DMB ligand in the lower axial position. Alternatively, the "base-off/HIS-on" family (e.g., methylmalonyl CoA mutase, MMCM)[12] displaces the lower axial base with a protein-derived histidine residue. The significance of this difference in cofactor binding scheme with regard to the enzymatic activation of the Co−C bond is an enduring subject of intense research.[13−18]

While not directly involved in catalysis, $Co^{2+}$corrinoid species are also formed upon accidental oxidation of the $Co^{+}$ intermediate of methyltransferases (e.g., methionine synthase and corrinoid iron−sulfur protein).[19] This "dead-end" species must be reductively reactivated in a process that is postulated to proceed through a cofactor state resembling $Co^{2+}$cobinamide ($Co^{2+}Cbi^{+}$) where the DMB ligand is replaced by a water molecule.[20−24] Similarly, the $Co^{+}$corrinoid:ATP adenosyltransferase (CobA) enzyme involved in the anaerobic biosynthesis of AdoCbl has been shown to proceed through a $Co^{2+}$ intermediate before the corrinoid substrate is further reduced to a highly nucleophilic $Co^{+}$ species capable of attacking the adenosyl group of the cosubstrate ATP.[25−28] In each case, the flavoproteins involved in the $Co^{2+} \rightarrow Co^{+}$ reduction step are unable to reduce free $Co^{2+}$corrinoids; therefore, the properties of the enzyme-bound cofactor must be tuned to shift the $Co^{2+/+}$ reduction potential into the physiologically accessible range. However, the mechanisms by which this enzyme-controlled redox tuning is achieved are largely unexplored.

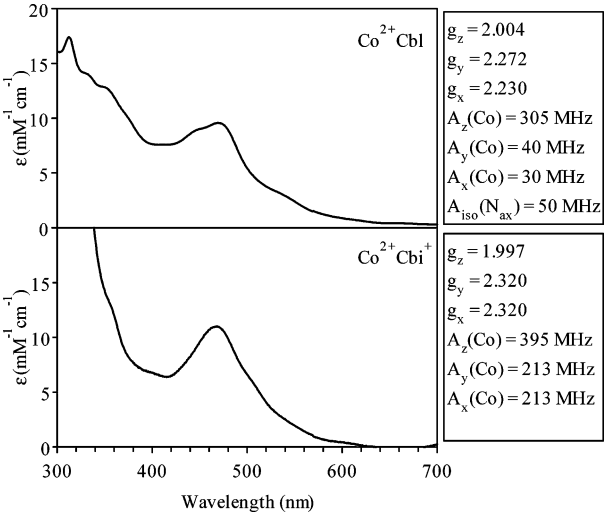


***Figure 2.*** Room-temperature Abs spectra (left) and relevant EPR parameters[29,30] (right) for $Co^{2+}$Cbl (top) and $Co^{2+}Cbi^{+}$ (bottom).

Spectroscopic studies of $Co^{2+}$Cbl (both free and bound to various enzymes) have been limited primarily to electronic absorption (Abs) and electron paramagnetic resonance (EPR) experiments. Figure 2 compares room-temperature Abs and relevant EPR parameters[29,30] from low-temperature studies of $Co^{2+}$Cbl (top) and $Co^{2+}Cbi^{+}$ (bottom). The Abs spectra of the two species are nearly identical except for a 4 nm blue-shift of the most intense feature from 474 nm for $Co^{2+}$Cbl to 470 nm for $Co^{2+}Cbi^{+}$. This modest shift is in striking contrast to the 65 nm blue-shift of the prominent Abs feature in the visible region and the drastic alteration of the absorption envelope upon displacement of the DMB in the lower axial position of AdoCbl

(9) Stich, T. A.; Brooks, A. J.; Buan, N. R.; Brunold, T. C. *J. Am. Chem. Soc.* **2003**, *125*, 5897−5914.
(10) Brooks, A. J.; Vlasie, M.; Banerjee, R.; Brunold, T. C. *J. Am. Chem. Soc.* **2004**, *126*, 8167−8180.
(11) Yamanishi, M.; Yamada, S.; Muguruma, Y.; Tobimatsu, T.; Ishida, A.; Yamauchi, J.; Toraya, T. *Biochemistry* **1998**, *37*, 4799−4803.
(12) Padmakumar, R.; Taoka, S.; Banerjee, R. *J. Am. Chem. Soc.* **1995**, *117*, 7033−7034.
(13) Dong, S. L.; Padmakumar, R.; Banerjee, R.; Spiro, T. G. *Inorg. Chim. Acta* **1998**, *270*, 392−398.
(14) Sirovatka, J. M.; Finke, R. G. *J. Am. Chem. Soc.* **1997**, *119*, 3057−3067.
(15) Chowdhury, S.; Banerjee, R. *Biochemistry* **1999**, *38*, 15287−15294.
(16) Brown, K. L.; Zou, X.; Li, J.; Chen, G. D. *Inorg. Chem.* **2001**, *40*, 5942−5947.
(17) Ishida, A.; Toraya, T. *Biochemistry* **1993**, *32*, 1535−1540.
(18) Dorweiler, J. S.; Finke, R. G.; Matthews, R. G. *Biochemistry* **2003**, *42*, 14653−14662.
(19) Matthews, R. G. *Acc. Chem. Res.* **2001**, *34*, 681−689.
(20) It should be noted that methionine synthase utilizes the complete MeCbl cofactor in the base-off/HIS-on conformation, whereas the corrinoid iron−sulfur protein employs a methylcobamide type cofactor that does not coordinate DMB or HIS.
(21) Base-off $Co^{2+}$Cbl and $Co^{2+}Cbi^{+}$ are spectroscopically indistinguishable by our techniques and are thus considered equivalent in the scope of this study.
(22) Banerjee, R. V.; Harder, S. R.; Ragsdale, S. W.; Matthews, R. G. *Biochemistry* **1990**, *29*, 1129−1135.
(23) Hall, D. A.; Jordan-Starck, T. C.; Loo, R. O.; Ludwig, M. L.; Matthews, R. G. *Biochemistry* **2000**, *39*, 10711−10719.
(24) Hall, D. A.; Kooi, C. W. V.; Stasik, C. N.; Stevens, S. Y.; Zuiderweg, E. R. P.; Matthews, R. G. *Proc. Natl. Acad. Sci. U.S.A.* **2001**, *98*, 9521−9526.
(25) Escalante-Semerena, J. C.; Suh, S. J.; Roth, J. R. *J. Bacteriol.* **1990**, *172*, 273−280.
(26) Rondon, M. R.; Trzebiatowski, J. R.; Escalante-Semerena, J. C. *Prog. Nucleic Acid Res. Mol. Biol.* **1997**, *56*, 347−384.
(27) Bauer, C. B.; Fonseca, M. V.; Holden, H. M.; Thoden, J. B.; Thompson, T. B.; Escalante-Semerena, J. C.; Rayment, I. *Biochemistry* **2001**, *40*, 361−374.
(28) Fonseca, M. V.; Escalante-Semerena, J. C. *J. Biol. Chem.* **2001**, *276*, 32101−32108.
(29) Van Doorslaer, S.; Jeschke, G.; Epel, B.; Goldfarb, D.; Eichel, R. A.; Krautler, B.; Schweiger, A. *J. Am. Chem. Soc.* **2003**, *125*, 5915−5927.
(30) Harmer, J.; Van Doorslaer, S.; Gromov, I.; Schweiger, A. *Chem. Phys. Lett.* **2002**, *358*, 8−16.

with a water molecule to generate $AdoCbi^+$. However, due to the lack of a suitable theoretical framework, which thus far has precluded assignments of key features in $Co^{2+}$corrinoid Abs spectra, the electronic origin of the much more dramatic effects of lower axial ligand substitution on the Abs spectrum of AdoCbl as compared to that of $Co^{2+}$Cbl remains unknown.

EPR spectroscopy has proved to be an invaluable tool when applied to $B_{12}$-dependent systems, as it is much more sensitive than Abs spectroscopy in detecting changes in the axial coordination environment of $Co^{2+}$corrinoids.[29−33] For example, EPR $g$ values and $^{59}$Co hyperfine parameters ($A_i$(Co)) for $Co^{2+}$Cbl and $Co^{2+}Cbi^+$, listed to the right of Figure 2, change markedly upon lower ligand substitution. Also shown are superhyperfine parameters ($A_{iso}(N_{ax})$) for $Co^{2+}$Cbl that reflect the interaction of the single unpaired electron in the Co $3d_{z^2}$-based MO and the coordinating $^{14}$N nucleus ($I = 1$) of the DMB ligand.[34] $Co^{2+}Cbi^+$ lacks an axial N-based ligand, and thus no $^{14}$N superhyperfine interaction is detected by EPR; however, recent multidimensional electron spin−echo envelope modulation (ESEEM) experiments confirm the presence of a solvent-derived water molecule in the lower axial position.[29] In addition to its sensitivity to axial ligand substitution, a further advantage of EPR spectroscopy over Abs spectroscopy is that it allows exclusive probing of $Co^{2+}$Cbl even in samples that are not completely converted to the $Co^{2+}$ state (both the $Co^{3+}$ and the $Co^+$ states of the cofactor are diamagnetic), a problem commonly experienced with $Co^{2+}$Cbl samples in general and for enzymatic species in particular.[12,35−37] Yet a major limitation of both EPR and ESEEM spectroscopies is that neither technique is adept at directly reporting the properties of the corrin ligand. In contrast, magnetic circular dichroism (MCD) spectroscopy potentially offers a probe that is both sensitive to axial bonding interactions as well as the geometric and electronic properties of the corrin ring moiety in $Co^{2+}$corrinoids.[9] Similar to EPR spectroscopy, MCD spectroscopy is particularly sensitive to paramagnetic chromophores and thus ideally suited for studying nonhomogeneous preparations of $Co^{2+}$corrinoids.[38] However, for MCD to be successfully employed in the study of $B_{12}$-dependent enzymes, it is essential that the electronic properties of the free $Co^{2+}$ containing corrinoids first be understood.

Density functional theory (DFT) and time-dependent DFT (TD-DFT) calculations on cofactor models possessing the full core of the corrin macrocycle have been used with great success to reproduce the relevant structural and electronic features as well as all key features in the experimental Abs spectra for a range of $Co^{3+}$corrinoids possessing vastly different axial ligands.[9,39−44] Building upon our free $Co^{3+}$corrinoid studies,[9] we have recently shown that quantitative interpretation of the spectroscopic data of AdoCbl within the framework of TD-DFT computations can provide detailed information concerning active site/cofactor interactions in the $B_{12}$-dependent enzyme MMCM.[10] Unfortunately, attempts to treat $Co^{2+}$corrinoids using similar computational methods are complicated by the open shell nature of the $Co^{2+}$ center. Nonetheless, calculations utilizing a local density approximation (LDA) DFT functional and zeroth-order relativistic approximation (ZORA) to the Hamiltonian have recently been shown to yield reasonable $g$ values as well as hyperfine and nuclear quadrupole parameters for various $Co^{2+}$corrinoid models,[29,30] demonstrating the potential of the DFT method for studying the electronic properties of free and enzyme-bound $Co^{2+}$corrinoid species.

In this paper, we present Abs, resonance Raman (RR), and, for the first time, MCD data of $Co^{2+}$Cbl and its derivative $Co^{2+}Cbi^+$. Spectroscopic data for both species are analyzed within the framework of TD-DFT calculations to assign the dominant features in the corresponding Abs and MCD spectra. The electronic origin for their nearly identical Abs spectra is explored on the basis of experimentally validated calculated electronic structure descriptions. These studies reveal that corrin-based $\pi \rightarrow \pi^*$ transitions that dominate the Abs spectra of $Co^{2+}$corrinoids are virtually unaffected by changes of the lower axial ligand, whereas transitions involving the $Co^{2+}$ 3d orbitals, which are observed for the first time here using MCD spectroscopy, are greatly perturbed by lower ligand substitution. Implications of our results with respect to the catalytic mechanism of Co−C bond activation and tuning of the $Co^{2+/+}$ redox couple employed by $B_{12}$-dependent enzymes are discussed.

## 2. Experimental Section

**Chemicals/Cofactors.** AdoCbl, aquacobalamin ($H_2OCbl^+$), dicyanocobinamide ($(CN)_2Cbi$), sodium borohydride ($NaBH_4$), sodium dithionite (DTH), and potassium formate (KCOOH) were purchased from Sigma and used as obtained. $AdoCbi^+$ was prepared enzymatically according to published procedures.[28] All solutions were degassed on a vacuum line and sparged with Ar gas. Base-on $Co^{2+}$cobalmin ($Co^{2+}$Cbl) samples were prepared by the following means: (i) chemical reduction of $H_2OCbl^+$ using DTH, (ii) reduction of $H_2OCbl^+$ with KCOOH, (iii) reduction of $H_2OCbl^+$ using the flavin system from *Salmonella enterica*,[28,45] and (iv) photolysis of AdoCbl in the presence of the radical trap TEMPO. While MCD spectra obtained on all $Co^{2+}$Cbl samples were nearly identical, only preparations (ii) and (iii) led to nearly complete conversion as needed for parallel characterization by Abs spectroscopy. $Co^{2+}Cbi^+$ samples were generated by (i) DTH reduction of $H_2OCbl^+$ at pH 2 (yielding base-off $Co^{2+}$Cbl),[21] (ii) KCOOH reduction of $AdoCbi^+$, and (iii) reduction of $(CN)_2Cbi$ with $NaBH_4$ at pH 7.[46] Identical MCD spectra were obtained for the various preparations of $Co^{2+}Cbi^+$, yet only preparation (ii) resulted in complete conversion.

**Spectroscopy.** Electronic Abs, CD, and MCD spectra were obtained using a Jasco J-715 spectropolarimeter in conjunction with an Oxford Instruments SM-4000 8T magnetocryostat. The samples used for low-temperature experiments were prepared under a $N_2$ atmosphere with

(31) Schrauzer, G. N.; Lee, L.-P. *J. Am. Chem. Soc.* **1968**, *90*, 6541−6543.
(32) Bayston, J. H.; Looney, F. D.; Pilbrow, J. R.; Winfield, M. E. *Biochemistry* **1970**, *9*, 2164−2172.
(33) Trommel, J. S.; Warncke, K.; Marzilli, L. G. *J. Am. Chem. Soc.* **2001**, *123*, 3358−3366.
(34) Pilbrow, J. R. In *$B_{12}$*; Dolphin, D., Ed.; Wiley: New York, 1982; pp 431−462.
(35) Huhta, M. S.; Chen, H. P.; Hemann, C.; Hille, C. R.; Marsh, E. N. G. *Biochem. J.* **2001**, *355*, 131−137.
(36) Seravalli, J.; Brown, K. L.; Ragsdale, S. W. *J. Am. Chem. Soc.* **2001**, *123*, 1786−1787.
(37) Ke, S.-C.; Torrent, M.; Museav, D. G.; Morokuma, K.; Warncke, K. *Biochemistry* **1999**, *38*, 12681−12689.
(38) MCD *C*-term contributions arise from species with paramagnetic ground states and dominate low-temperature MCD spectra.
(39) Dolker, N.; Maseras, F.; Lledos, A. *J. Phys. Chem. B* **2001**, *105*, 7564−7571.
(40) Dolker, N.; Maseras, F.; Lledos, A. *J. Phys. Chem. B* **2002**, *106*, 8910−8910.
(41) Jensen, K. P.; Sauer, S. P. A.; Liljefors, T.; Norrby, P. O. *Organometallics* **2001**, *20*, 550−556.
(42) Jensen, K. P.; Ryde, U. *J. Mol. Struct. (THEOCHEM)* **2002**, *585*, 239−255.
(43) Kozlowski, P. M. *Curr. Opin. Chem. Biol.* **2001**, *5*, 736−743.
(44) Andruniow, T.; Kozlowski, P. M.; Zgierski, M. Z. *J. Chem. Phys.* **2001**, *115*, 7522−7533.
(45) Fonseca, M. V.; Escalante-Semerena, J. C. *J. Bacteriol.* **2000**, *182*, 4304−4309.
(46) $Co^{2+}Cbi^+$ is known to bind $CN^-$ only at pH > 11 (see ref 32).

60% (v/v) glycerol added to ensure glass formation upon freezing. Sample concentrations ranged from 0.15 to 0.8 mM and were determined spectrophotometrically at 300 K on the basis of published molar extinction coefficients.[47,48] All MCD spectra reported in this paper were obtained by subtracting the −7 T spectrum from the +7 T spectrum to eliminate the natural CD contributions.

RR spectra were obtained upon excitation with a Coherent I-305 $Ar^+$ ion laser (between 351 and 514 nm) with 10−50 mW laser power at the sample. The scattered light was collected using a ∼135° backscattering arrangement, dispersed by an Acton Research triple monochromator (equipped with 300, 1200, and 2400 grooves/mm gratings), and analyzed with a Princeton Instruments Spec X: 100BR deep depletion, back-thinned CCD camera. $Co^{2+}$Cbl samples for RR experiments were prepared in NMR tubes by reduction of $H_2OCbl^+$ using KCOOH. Spectra were accumulated at 77 K by placing the sample in an EPR dewar filled with liquid $N_2$ to prevent sample degradation during data collection. RR excitation profiles were obtained by quantifying the peak intensities relative to the ice peak at 228 $cm^{-1}$. All RR excitation profiles shown in this study represent the average of at least three independent data sets.

**Computational Models.** While many different approaches can be devised to generate suitable models for computational studies of corrinoid species,[40−42,49−51] we employed here the methodology developed in our $Co^{3+}$corrinoid studies;[9] that is, our $Co^{2+}$corrinoid models were evaluated on the basis of spectroscopic data using the TD-DFT method to predict the corresponding Abs spectra. A set of three distinct $Co^{2+}$Cbl models were derived: (i) from available X-ray data[47] (termed model **Cbl-I**), (ii) by full geometry optimization using a pure DFT functional (**Cbl-II**), and (iii) by full optimization using the three-parameter hybrid density functional B3LYP (**Cbl-III**). In each case, the DMB base was modeled by an imidazole,[52] where for **Cbl-I** the Co−N bond length and relative orientation of the five-membered ring of the base were preserved and the entire nucleotide loop was replaced by an H atom at $C^{17}$ (see Figure 1). All other corrin ring substituents were replaced by H atoms separated by 1.08 Å from the neighboring C atoms. These types of modifications of the native corrin ring structure were shown previously to have little effect on the electronic structure of $Co^{3+}$Cbl models.[9] Geometry optimizations using pure DFT to generate the model **Cbl-II** were carried out on a cluster of 20 Pentium Xeon nodes emplying the Amsterdam Density Functional (ADF) 2003.02 suite of programs.[53,54] These calculations were performed using the Vosko−Wilk−Nusair local density approximation (VWN-LDA)[55] with the nonlocal gradient corrections of Becke for exchange[56] and Perdew for correlation[57] employing ADF basis set II (a double-ζ STO basis for valence levels) and an integration constant of 4.0. Core orbitals were frozen through 1s (O, N, C) and 3p (Co). Geometry optimization of **Cbl-III** was carried out on a desktop PC using the ORCA 2.2 software package developed by Dr. Frank Neese (MPI Mülheim, Germany)[58] employing Becke's three-parameter hybrid functional for exchange[59,60] along with the Lee−Yang−Parr correlation functional[61] (B3LYP) and the default amount of 20% Hartree−Fock exchange. All atoms were treated with the SV(P) (Ahlrichs polarized split valence) basis[62] in conjunction with the SV/C auxiliary basis[63] except for cobalt which was treated using the larger TZVP (Ahlrichs polarized triple-ζ valence) basis.[64] The size of the integration grid was set to 3 (Lebedev 194 points) in all cases.

$Co^{2+}Cbi^+$ models were generated following the same general guidelines described above for $Co^{2+}$Cbl. However, as structural data for $Co^{2+}Cbi^+$ are not yet available, **Cbi-I** was derived from the **Cbl-I** model with the axial base replaced by a water molecule. The position of the water ligand was optimized by spin-unrestricted DFT energy minimization using ADF, while all other atoms were kept frozen. Atomic coordinates of all $Co^{2+}$Cbl and $Co^{2+}Cbi^+$ models discussed in the text are included in the Supporting Information (Tables S1−S6).

**Single-Point DFT Calculations.** All single-point DFT calculations were carried out using the ORCA 2.2 software package. Following the methodology developed in our previous work,[9] pure DFT and B3LYP calculations were performed on all $Co^{2+}$Cbl and $Co^{2+}Cbi^+$ models. Spin-unrestricted calculations using the Perdew−Wang LDA (PW-LDA)[65] with the gradient corrections by Becke[66] and Perdew[57] were employed with the DGauss (Gaussian polarized double-ζ valence orbital) basis[67] along with the Demon/J auxiliary basis.[68] Hybrid B3LYP calculations were performed using the same basis sets and parameters as described above. Isosurface plots of molecular orbitals were generated with the gOpenMol program developed by Laaksonen[69,70] using an isodensity value of 0.03 $b^{-3}$.

**TD-DFT Calculations.** Vertical excitation energies and transition dipole moments for all $Co^{2+}$Cbl and $Co^{2+}Cbi^+$ models were calculated by the TD-DFT method[71−73] within the Tamm−Dancoff approximation[74,75] as implemented in ORCA 2.2, employing both the LDA (TD-DFT/PW) and the hybrid (TD-DFT/B3LYP) functionals with the corresponding basis sets as described above. Convergence of TD-DFT calculations required that the resolution of the identity approximation be used in calculating the Coulomb term.[76] In each case, at least 60 excited states were calculated by including all one-electron excitations within an energy window of ±3 hartrees with respect to the HOMO/LUMO energies. As the TD-DFT formalism expresses each transition in terms of a linear combination of one-electron excitations between occupied and virtual molecular orbitals, it often becomes difficult to assess the precise nature of the corresponding excited state. Therefore, to aid in the interpretation and assignment of transitions, changes in electron density distribution upon excitation were visualized by plotting electron density difference maps (EDDMs). These plots were generated with the gOpenMol program[69,70] using an isodensity value of 0.003 $b^{-3}$.

**EPR Parameter Calculations.** Molecular *g* values and hyperfine parameters for the cobalt center, all corrin ring nitrogens, and the coordinating atoms of axial ligands were calculated with the ORCA program by solving the coupled-perturbed SCF (CP-SCF) equations[77]


(47) Kräutler, B.; Keller, W.; Kratky, C. *J. Am. Chem. Soc.* **1989**, *111*, 8936−8938.
(48) Hay, B. P.; Finke, R. G. *J. Am. Chem. Soc.* **1987**, *109*, 8012−8018.
(49) Andruniow, T.; Zgierski, M. Z.; Kozlowski, P. M. *Chem. Phys. Lett.* **2000**, *331*, 509−512.
(50) Andruniow, T.; Zgierski, M. Z.; Kozlowski, P. M. *J. Am. Chem. Soc.* **2001**, *123*, 2679−2680.
(51) Randaccio, L.; Geremia, S.; Stener, M.; Toffoli, D.; Zangrando, E. *Eur. J. Inorg. Chem.* **2002**, 93−103.
(52) The structural parameters of the imidazole modeling the DMB base were obtained from a full geometry optimization of the $H_2OCbl^+$ model described in ref 9.
(53) Baerends, E. J.; Ellis, D. E.; Ros, P. *Chem. Phys.* **1973**, *2*, 41−51.
(54) te Velde, G.; Baerends, E. J. *J. Comput. Phys.* **1992**, *99*, 84−98.
(55) Vosko, S. H.; Wilk, L.; Nusair, M. *Can. J. Phys.* **1980**, *58*, 1200−1211.
(56) Becke, A. D. *Phys. Rev. A* **1988**, *38*, 3098−3100.
(57) Perdew, J. P. *Phys. Rev. B* **1986**, *33*, 8822−8824.
(58) Neese, F.; Solomon, E. I. *Inorg. Chem.* **1999**, *38*, 1847−1865.
(59) Becke, A. D. *J. Chem. Phys.* **1993**, *98*, 1372−1377.
(60) Becke, A. D. *J. Chem. Phys.* **1993**, *98*, 5648−5652.
(61) Lee, C.; Yang, W.; Parr, R. G. *Phys. Rev. B* **1988**, *37*, 785−789.
(62) Schäfer, A.; Horn, H.; Ahlrichs, R. *J. Chem. Phys.* **1992**, *97*, 2571−2577.
(63) The Ahlrichs auxiliary basis sets were obtained from the TurboMole basis set library under ftp://ftp.chemie.uni-karlsruhe.de/pub/cbasen. Weigend, F.; Häser, M. *Theor. Chem. Acc.* **1997**, *97*, 331−340.
(64) Schäfer, A.; Huber, C.; Ahlrichs, R. *J. Chem. Phys.* **1994**, *100*, 5829−5835.
(65) Perdew, J. P.; Wang, Y. *Phys. Rev. B* **1992**, *45*, 13244−13249.
(66) Becke, A. D. *J. Chem. Phys.* **1986**, *84*, 4524−4529.
(67) Andzelm, J.; Wimmer, E. *J. Chem. Phys.* **1992**, *96*, 1280−1303.
(68) Godbout, N.; Salahub, D. R.; Andzeim, J.; Wimmer, E. *Can. J. Chem.* **1992**, *70*, 560−571.
(69) Laaksonen, L. *J. Mol. Graphics* **1992**, *10*, 33−34.
(70) Bergman, D. L.; Laaksonen, L.; Laaksonen, A. *J. Mol. Graphics Modell.* **1997**, *15*, 301−306.
(71) Bauernschmitt, R.; Ahlrichs, R. *Chem. Phys. Lett.* **1996**, *256*, 454−464.
(72) Casida, E. M.; Jamorski, C.; Casida, K. C.; Salahub, D. R. *J. Chem. Phys.* **1998**, *108*, 4439−4449.
(73) Stratmann, R. E.; Scuseria, G. E.; Frisch, M. J. *J. Chem. Phys.* **1998**, *109*, 8218−8224.
(74) Hirata, S.; Head-Gordon, M. *Chem. Phys. Lett.* **1999**, *302*, 375−382.
(75) Hirata, S.; Head-Gordon, M. *Chem. Phys. Lett.* **1999**, *314*, 291−299.
(76) Neese, F.; Olbrich, G. *Chem. Phys. Lett.* **2002**, *362*, 170−178.

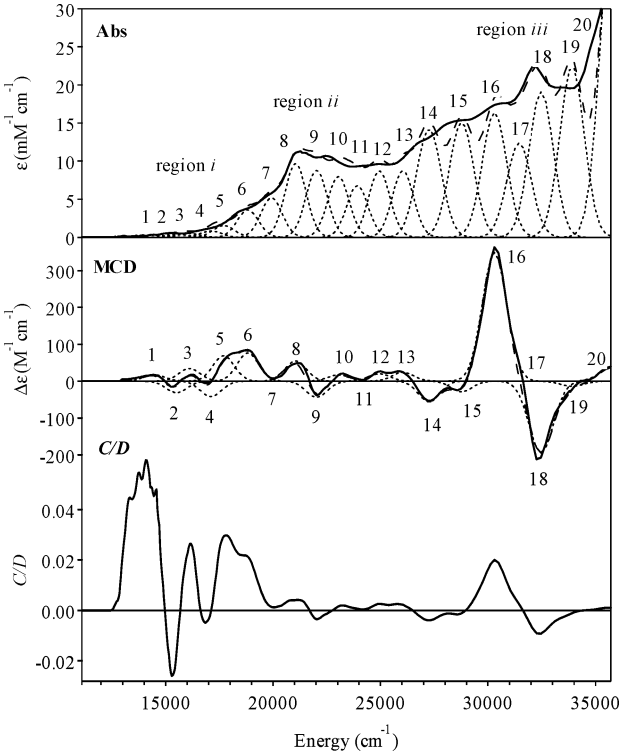


***Figure 3.*** Solid lines: Absorption (top) and 7 T MCD (center) spectra at 4.5 K of $Co^{2+}$Cbl generated by reducing $H_2OCbl^+$ with the flavin system from *S. enterica*. Dotted lines: Gaussian deconvolutions of the experimental spectra. Dashed lines: Sum of individual Gaussian bands. The fit parameters are given in Table 1. The *C*/*D* ratio is presented in the bottom panel.

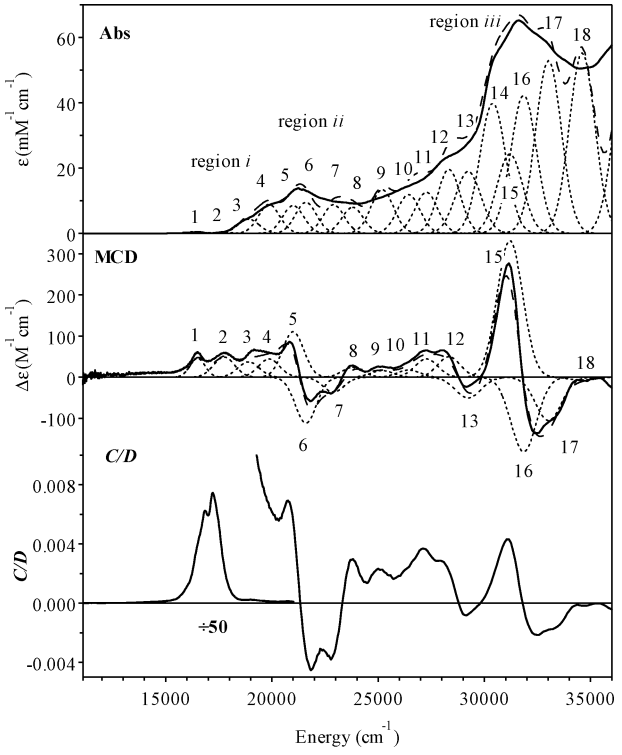


***Figure 4.*** Solid lines: Absorption (top) and 7 T MCD (center) spectra at 4.5 K of $Co^{2+}Cbi^+$ generated by the reduction of $AdoCbi^+$ with KCOOH. Dotted lines: Gaussian deconvolutions of the experimental spectra. Dashed lines: Sum of individual Gaussian bands. The fit parameters are given in Table 1. The *C*/*D* ratio is presented in the bottom panel.

and employing both the PW-LDA functional and the hybrid B3LYP functional. In each case, the "core-properties" with extended polarization (CP(PPP)) basis[78] and Kutzelnigg's NMR/EPR (IGLOIII) basis[79] were used to treat the cobalt center and all metal-ligating atoms (N and O), respectively, while the same basis sets described above were used for all other atoms. The CP-SCF calculations of the *g* values included all orbitals within a ±100 hartree window of the HOMO/LUMO energies with the origin of the **g**-"tensor" defined by the center of electronic charge of the model. A high-resolution radial grid with an integration accuracy of 7 was used on atoms for which the hyperfine parameters were calculated. Spin−orbit coupling contributions were included in the calculation of the $^{59}$Co hyperfine tensor.[80]

## 3. Results and Analysis

**3.1. Spectroscopic Data. (i) Abs and MCD.** Electronic absorption (Abs) and magnetic circular dichroism (MCD) spectra of $Co^{2+}$Cbl and $Co^{2+}Cbi^+$ are shown in Figures 3 and 4, respectively. Comparison of these two data sets affords unique insight into the subtle differences in the electronic structures of two $Co^{2+}$corrinoids that only differ with respect to the identity of the lower ligand, a pendant dimethylbenzimidazole (DMB) in the case of base-on $Co^{2+}$Cbl and a $H_2O$ molecule in $Co^{2+}Cbi^+$. Consistent with the paramagnetic $S = {}^1/_2$ ground state of these low-spin $Co^{2+}$ species, all features in the MCD spectra of Figures 3 and 4 are temperature dependent (not shown), exhibiting saturation behavior as predicted by the $S = {}^1/_2$ Brillouin curve.[81] The Abs spectra of both $Co^{2+}$corrinoid species are dominated by intense features centered in the visible region (region ii) presumably due to corrin-centered $\pi \rightarrow \pi^*$ (cor $\pi \rightarrow \pi^*$) transitions.[82,83] Low-energy ligand field (d → d) transitions are formally parity forbidden and thus carry little intensity in Abs spectra. However, through the mechanism of spin−orbit coupling, these transitions typically acquire significant MCD intensity. Therefore, the ratio of MCD and Abs signal intensities, expressed by the *C*/*D* ratio, provides a qualitative measure of the metal d-orbital character involved in each electronic transition. *C*/*D* ratios greater than ∼0.03 are indicative of d → d transitions, whereas smaller ratios are characteristic of charge transfer or $\pi \rightarrow \pi^*$ transitions.[81]

Abs and MCD spectra of the $Co^{2+}$corrinoid species included in this study (Figures 3 and 4) were iteratively fit with the fewest possible number of Gaussian bands to resolve the major electronic transitions contributing to the spectral region between 10 000 and 35 000 $cm^{-1}$. The relevant results from these Gaussian deconvolutions are summarized in Table 1 and will be discussed next.

**$Co^{2+}$Cbl.** The $Co^{2+}$Cbl Abs spectrum (Figure 3, top) is dominated by a broad feature in the visible region between 20 000 and 26 000 $cm^{-1}$ (region ii) with a maximum at 21 100 $cm^{-1}$ (474 nm). Spectral deconvolution of the MCD spectrum of region ii requires five Gaussians (bands 8−10, 12, and 13); however, two additional Gaussians (bands 7 and 11) are

(77) Neese, F. *J. Chem. Phys.* **2001**, *115*, 11080−11096.
(78) Neese, F. *Inorg. Chim. Acta* **2002**, *337*, 181−192.
(79) Kutzelnigg, W.; Fleischer, U.; Schindler, M. *The IGLO Method: Ab Initio Calculation and Interpretation of NMR Chemical Shifts and Magnetic Susceptibilities*; Springer-Verlag: Heidelberg, 1990; Vol. 23.
(80) Neese, F. *J. Chem. Phys.* **2003**, *118*, 3939−3948.
(81) Pavel, E. G.; Solomon, E. I. In *Spectroscopic Methods in Bioinorganic Chemistry*; Solomon, E. I., Hodgson, K. O., Eds.; American Chemical Society; Distributed by Oxford University Press: Washington, DC [New York], 1998; pp 119−135.
(82) Firth, R. A.; Hill, H. A. O.; Pratt, J. M.; Williams, R. J. P.; Jackson, W. R. *Biochemistry* **1967**, *6*, 2178−2189.
(83) Pratt, J. M. In *Chemistry and Biochemistry of $B_{12}$*; Banerjee, R., Ed.; Wiley: New York, 1999; pp 113−164.

***Table 1.*** Fit Parameters from Gaussian Deconvolutions of the Abs and MCD Spectra of $Co^{2+}$Cbl and $Co^{2+}Cbi^{+}$ (Figures 3 and 4)

| corrinoid | band | energy ($cm^{-1}$) | $\epsilon$(Abs) ($M^{-1}cm^{-1}$) | $\Delta\epsilon$(MCD) ($M^{-1}cm^{-1}$) | *C*/*D* |
|---|---|---|---|---|---|
| $Co^{2+}$Cbl | 1 | 14 470 | 300 | 17.1 | 0.055 |
| | 2 | 15 510 | 400 | −31.4 | −0.075 |
| | 3 | 16 110 | 500 | 34.2 | 0.065 |
| | 4 | 17 110 | 810 | −41.6 | −0.049 |
| | 5 | 17 700 | 1550 | 68.8 | 0.042 |
| | 6 | 18 830 | 3600 | 76.1 | 0.020 |
| | 7 | 19 930 | 5160 | 0.0 | 0.000 |
| | 8 | 21 050 | 9690 | 54.6 | 0.005 |
| | 9 | 22 030 | 8780 | −43.8 | −0.005 |
| | 10 | 23 040 | 7990 | 16.9 | 0.002 |
| | 11 | 23 930 | 6790 | 0.0 | 0.000 |
| | 12 | 24 950 | 8720 | 19.6 | 0.002 |
| | 13 | 26 040 | 8750 | 24.0 | 0.003 |
| | 14 | 27 260 | 14 210 | −55.8 | −0.004 |
| | 15 | 28 770 | 15 080 | −29.0 | −0.002 |
| | 16 | 30 300 | 16 380 | 348.6 | 0.020 |
| | 17 | 31 450 | 12 420 | 0.0 | 0.000 |
| | 18 | 32 470 | 19 080 | −194.1 | −0.010 |
| | 19 | 33 910 | 22 050 | −13.6 | −0.001 |
| | 20 | 35 770 | 40 900 | 36.8 | 0.001 |
| $Co^{2+}Cbi^{+}$ | 1 | 16 500 | 450 | 45.9 | 0.098 |
| | 2 | 17 750 | 300 | 49.0 | 0.156 |
| | 3 | 18 900 | 4350 | 37.3 | 0.008 |
| | 4 | 19 870 | 8900 | 44.3 | 0.005 |
| | 5 | 21 000 | 8500 | 110.9 | 0.012 |
| | 6 | 21 600 | 9500 | −111.4 | −0.011 |
| | 7 | 22 900 | 8800 | −36.3 | −0.004 |
| | 8 | 23 800 | 8000 | 24.0 | 0.003 |
| | 9 | 25 190 | 13 400 | 16.0 | 0.001 |
| | 10 | 26 440 | 11 910 | 17.5 | 0.001 |
| | 11 | 27 270 | 12 640 | 44.6 | 0.003 |
| | 12 | 28 330 | 19 260 | 49.6 | 0.002 |
| | 13 | 29 240 | 18 990 | −50.5 | −0.003 |
| | 14 | 30 390 | 40 000 | 0.0 | 0.000 |
| | 15 | 31 200 | 24 330 | 332.6 | 0.013 |
| | 16 | 31 850 | 42 350 | −181.6 | −0.004 |
| | 17 | 33 020 | 52 910 | −105.6 | −0.002 |
| | 18 | 34 600 | 55 270 | −6.9 | 0.000 |

necessary to obtain a satisfactory fit of the Abs spectrum (Table 1). Band 8, which dominates the Abs spectrum in this region, is relatively weak in the MCD spectrum and consequently possesses a small *C*/*D* ratio of $\leq 0.01$ (Figure 3, bottom; Table 1). This result considered along with resonance Raman data presented below indicate that the corresponding transition involves molecular orbitals that possess significant corrin $\pi/\pi^*$ character. Interestingly, bands 8 and 9 form a derivative-shaped feature in the MCD spectrum centered at 21 500 $cm^{-1}$ that exhibits a somewhat different temperature dependence than all of the other features (Figure S2), losing intensity with increasing temperature more slowly than predicted by the $S = {}^1/_2$ Brillouin curve. This finding suggests that an authentic *A*-term mechanism involving an orbitally degenerate excited state may contribute to the observed intensity.[81]

On its low-energy side, the central feature is accompanied by several weaker bands between 10 000 and 20 000 $cm^{-1}$ (region i). Gaussian deconvolution of the $Co^{2+}$Cbl MCD spectrum (Figure 3, center; Table 1) resolves six bands (designated bands 1−6) in region i of which the first four display large *C*/*D* ratios (Figure 3, bottom), suggesting that the corresponding transitions possess significant $Co^{2+}$ d → d character. The Abs envelope above 26 000 $cm^{-1}$ (region iii) is composed of several poorly resolved intense features, reminiscent of the distorted $\gamma$-region observed in the "unique" Abs spectra of alkyl-$Co^{3+}$Cbls (e.g., AdoCbl and MeCbl).[9] While a single peak centered at 32 470 $cm^{-1}$ is resolved in region iii of the Abs spectrum, analysis of the MCD spectrum (Figure 3, center; Table 1) reveals the presence of at least seven transitions (bands 14−20) in this region. The two most intense MCD features appear as a derivative shaped pseudo-*A* term that crosses the zero-axis at 31 800 $cm^{-1}$. The relatively large *C*/*D* ratio (Figure 3, bottom) suggests that the corresponding electronic transitions involve molecular orbitals that possess significant $Co^{2+}$ 3d orbital character, while their large intensities in the Abs spectrum imply considerable involvement of corrin $\pi/\pi^*$ orbitals.

**$Co^{2+}Cbi^{+}$.** As for $Co^{2+}$Cbl discussed above, the Abs spectrum of $Co^{2+}Cbi^{+}$ (Figure 4, top) can be divided into three regions centered about the dominant feature in the visible region at 21 275 $cm^{-1}$ (470 nm). This most prominent peak in region ii of the $Co^{2+}Cbi^{+}$ Abs spectrum (bands 5 and 6) exhibits a small *C*/*D* ratio and is blue-shifted by 175 $cm^{-1}$ (4 nm) relative to the corresponding feature in the $Co^{2+}$Cbl Abs spectrum (band 8; Table 1).

Although no Abs features are resolved in region i below 20 000 $cm^{-1}$, Gaussian deconvolution of the $Co^{2+}Cbi^{+}$ MCD spectrum (Figure 4, center) reveals that at least four electronic transitions contribute to this region (bands 1−4). The large corresponding *C*/*D* ratios (Figure 4, bottom) suggest that these transitions are likely $Co^{2+}$ d → d in character. Note that in the $Co^{2+}$Cbl spectrum these transitions are considerably red-shifted (cf., Figures 3 and 4; Table 1). Thus, substitution of the axial ligand DMB (a moderately strong $\sigma$-donor) with the rather weakly electron-donating water molecule in $Co^{2+}Cbi^{+}$ has a large effect on the energies of the $Co^{2+}$ d → d transitions, which provides an interesting contrast to the modest shift observed for the central feature in region ii.

The near UV region of the Abs spectrum (region iii, bands 14−18) is dominated by a broad feature with a maximum at 31 800 $cm^{-1}$ that coincides with the crossing point of the intense pseudo *A*-term in the MCD spectrum (note that the negatively signed component of this pseudo *A*-term is actually composed of three Gaussians, bands 16−18). Interestingly, these features are very similar in energy and general appearance to those observed in the MCD spectrum of $Co^{2+}$Cbl, indicating that the corresponding sets of electronic transitions are insulated from the perturbing effects of lower axial ligand substitution.

The experimental data presented in Figures 3 and 4 demonstrate the dramatically enhanced sensitivity of MCD spectroscopy over Abs spectroscopy in probing the subtle changes in electronic structure of $Co^{2+}$corrinoids accompanying lower axial ligand substitution. Importantly, our MCD data reveal that while the energies of transitions involving the corrin ligand (i.e., cor $\pi \rightarrow \pi^*$ transitions) are only modestly perturbed from $Co^{2+}$Cbl to $Co^{2+}Cbi^{+}$, the $Co^{2+}$ d → d transitions are considerably more sensitive to changes in the coordination environment of the Co center.

**(ii) RR Data.** The RR spectrum of $Co^{2+}$Cbl obtained upon laser excitation at 20 986 $cm^{-1}$ (476.5 nm) is shown in Figure 5 (top). This spectrum is qualitatively very similar to those reported for $Co^{3+}$corrinoids in that it is also dominated by several very intense peaks between 1000 and 1600 $cm^{-1}$ that can be attributed to corrin-based normal modes involving primarily C═C stretching motion.[84−87] The RR excitation profile

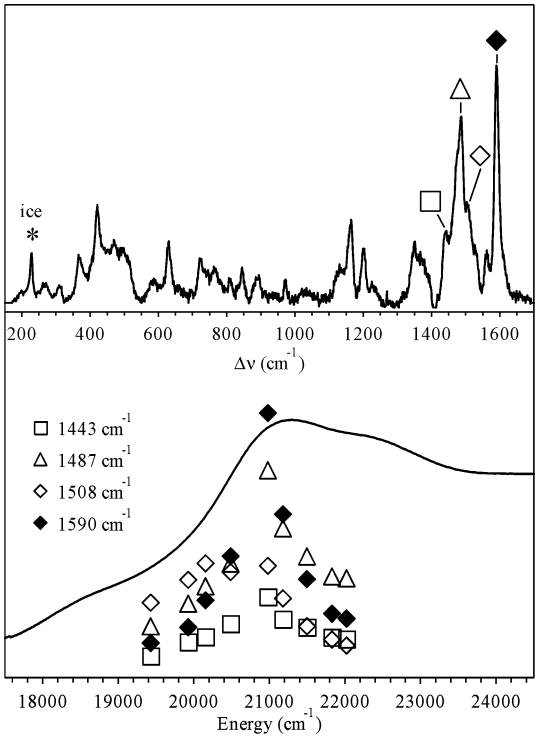


***Figure 5.*** Top: 476.5 nm (20 986 $cm^{-1}$) excited RR spectrum of $Co^{2+}$Cbl at 77 K. Bottom: Room-temperature Abs spectrum of $Co^{2+}$Cbl (solid line) and 77 K RR excitation profile data for corrin ring modes at 1443 (□), 1487 (△), 1508 (◇), and 1590 (◆) $cm^{-1}$.

data for $Co^{2+}$Cbl (Figure 5, bottom) show simultaneous enhancement of the prominent peaks centered at 1443, 1487, and 1590 $cm^{-1}$ (Figure 5, top) upon laser excitation in region ii of the Abs spectrum. In each case, the enhancement profile roughly traces the Abs envelope, indicating that the electronic transitions contributing to region ii of the Abs spectrum give rise to large excited state distortions of the corrin ring, in support of our assignment of these transitions as being primarily cor $\pi \rightarrow \pi^*$ in character.

For $Co^{3+}$corrinoids, polarization information for electronic transitions has previously been obtained through examination of the enhancement behavior of two perpendicularly polarized corrin ring stretching modes, that is, the long-axis ($\nu_{LA}$) and short-axis ($\nu_{SA}$) modes, which involve symmetric stretching of the C═C double bonds along the $C^5\cdots C^{15}$ and $Co\cdots C^{10}$ vectors of the corrin ring (Figure 1), respectively.[9,86,88,89] In each case, preferential enhancement of $\nu_{LA}$ was observed in resonance with the so-called α-band that arises from the lowest-energy cor $\pi \rightarrow \pi^*$ transition. Presumably, $Co^{2+}$corrinoids also possess long-axis and short-axis polarized corrin ring stretching modes; however, interpretation of $Co^{2+}$Cbl RR profile data is complicated by the simultaneous enhancement of several corrin modes for excitation in region ii. This enhancement pattern suggests that the corresponding electronic transitions are polarized intermediately between the short-axis and long-axis vectors and/or that several electronic transitions of varying polarizations occur in close energetic proximity to one another. Support for the latter scenario is provided by our MCD data, as observation of the derivative-shaped pseudo *A*-term feature in region ii (Figure 3, center) requires that the corresponding transitions be differently polarized.

Interestingly, a corrin-based mode at 1508 $cm^{-1}$ exhibits two maxima in the RR excitation profile at 20 200 and 21 000 $cm^{-1}$ (Figure 5, ◇), possibly suggesting that the cor $\pi \rightarrow \pi^*$-based electronic transitions at lower energy give rise to excited state distortion primarily along this coordinate. However, given the similar frequency of this mode and $\nu_{LA}$ of $H_2OCbl^+$,[9,86] we cannot rule out that the 1508 $cm^{-1}$ feature in the $Co^{2+}$Cbl RR spectrum derives from a small percentage of the starting material. Nevertheless, our preliminary studies indicate that the peak at 1508 $cm^{-1}$ is sensitive to deuterium labeling at $C^{10}$ of the corrin ring (i.e., employing the method of acid-catalyzed corrin ring deuterium labeling at $C^{10}$ developed by Puckett et al.,[90] we observed a 3.5 $cm^{-1}$ downshift of the 1508 $cm^{-1}$ mode and no shift for the 1487 $cm^{-1}$ mode), suggesting that it arises from a short-axis polarized corrin ring vibration of $Co^{2+}$Cbl. The relative intensities of these high-energy features exhibited slight variations among different samples, yet a red-shift by 3.5 $cm^{-1}$ of the 1508 $cm^{-1}$ peak was consistently observed for all deuterated $Co^{2+}$Cbl samples investigated.

**3.2. Computational Data.** Few computational studies of $Co^{2+}$corrinoids have been reported to date, and, so far, none has attempted to elucidate the natures of the electronic excited states and their relationship to those of $Co^{3+}$corrinoids.[29,42] Although hampered by the size of the system as well as the open shell nature of the $Co^{2+}$ center, considerable success has been achieved in describing certain aspects of the $Co^{2+}$corrinoid electronic structure using DFT computations. The validity of past calculations was gauged primarily on agreement with available EPR data and whether the calculation arrived at the appropriate ground-state description, that the unpaired electron resides in a Co $3d_{z^2}$-based MO. Generally, the latter criterion was always met, while success to meet the former varied considerably depending on the model and computational method employed. As the actual corrin ring conformation presumably has a small effect on the calculation of the aforementioned properties, validation of the $Co^{2+}$corrinoid models on the basis of EPR data alone appears insufficient. Therefore, we have generated three distinct models for each $Co^{2+}$corrinoid species investigated here and used both the electronic Abs and the EPR data to evaluate these models.

Our previous work on $Co^{3+}$Cbls demonstrated that truncated models derived from crystal structure coordinates are beneficial in that they preserve the actual conformation of the corrin ring by accounting for structural features not explicitly included in our models.[9] The same approach was adopted in this study; however, the lack of structural data for $Co^{2+}Cbi^+$ prompted us to examine a wider range of $Co^{2+}$corrinoid models, including some generated by full DFT geometry optimization. In the following section, all models examined are presented and evaluated on the basis of experimental data.

**Evaluation Process.** Three different $Co^{2+}$Cbl models (subsequently referred to as models **Cbl-I**−**III**) were obtained by

(84) Mayer, E.; Gardiner, D. J.; Hester, R. E. *J. Chem. Soc., Faraday Trans. 2* **1973**, *69*, 1350−1358.
(85) Wozniak, W. T.; Spiro, T. G. *J. Am. Chem. Soc.* **1973**, *95*, 3402−3404.
(86) Salama, S.; Spiro, T. G. *J. Raman Spectrosc.* **1977**, *6*, 57−60.
(87) Nie, S. M.; Marzilli, P. A.; Marzilli, L. G.; Yu, N. T. *J. Am. Chem. Soc.* **1990**, *112*, 6084−6091.
(88) Mayer, E.; Gardiner, D. J.; Hester, R. E. *Mol. Phys.* **1973**, *26*, 783−787.
(89) Galluzzi, F.; Garozzo, M.; Ricci, F. F. *J. Raman Spectrosc.* **1974**, *2*, 351−362.
(90) Puckett, J. M.; Mitchell, M. B.; Hirota, S.; Marzilli, L. G. *Inorg. Chem.* **1996**, *35*, 4656−4662.

(i) using crystal structure coordinates of $Co^{2+}$Cbl, (ii) full geometry optimization using a pure DFT functional, and (iii) full geometry optimization using the B3LYP hybrid functional (see Experimental Section for details). The same procedure was adopted to generate models for $Co^{2+}Cbi^{+}$ (**Cbi-I**−**III**) except that in case (i) the corrin ring from the $Co^{2+}$Cbl crystal structure was used and the axial water ligand position was optimized using pure DFT with all other atoms kept frozen. The full geometry optimizations performed on the $Co^{2+}$Cbl model consistently led to a flattening of the corrin ring, from 16.3° (**Cbl-I** and X-ray data[47]) to 6.8° (**Cbl-II**) and 13.6° (**Cbl-III**), as expected because the bulky DMB was modeled by a sterically less demanding imidazole. Nevertheless, the optimized metal−ligand bond lengths and calculated bond orders are virtually identical for all three models. The fully optimized models of $Co^{2+}Cbi^{+}$ exhibited a greater flattening of the ring from 16.3° (**Cbi-I**) to 5.1° (**Cbi-II**) and 5.7° (**Cbi-III**), consistent with a further decrease in bulkiness from imidazole to water. However, as **Cbi-I** is not based on crystal structure data, the corrin ring conformation in this model does not necessarily reflect the structural constraints imposed by the outer ring substituents in the actual $Co^{2+}Cbi^{+}$ cofactor. As a result of this increased spread in corrin ring conformations, models for $Co^{2+}Cbi^{+}$ exhibited a more pronounced variation in axial ligand bond length in comparison to that noted above for $Co^{2+}$Cbl, with the Co−$OH_2$ bond lengthening from 2.201 to 2.231 and 2.286 Å for each successive model. However, all models are reasonably consistent with the Co−$OH_2$ bond distance of 2.22 Å determined experimentally by EXAFS spectroscopy.[91]

Two sets of TD-DFT calculations were performed on each $Co^{2+}$corrinoid model: one using the PW-LDA functional (TD-DFT/PW) and the other employing the B3LYP hybrid functional (TD-DFT/B3LYP). Figure 6 compares TD-DFT predicted Abs spectra for all three $Co^{2+}$Cbl models considered to the corresponding experimental spectrum (see Figure S1 for a similar comparison of experimental and TD-DFT-computed $Co^{2+}Cbi^{+}$ Abs data). To facilitate this comparison, the TD-DFT-calculated transition energies and oscillator strengths were used to simulate Abs spectra assuming that each electronic transition gives rise to a Gaussian band with full width at half-maximum of $\nu_{1/2} = 1250\ cm^{-1}$. Under this assumption, the predicted oscillator strength ($f_{osc}$) and computed molar extinction coefficient $\epsilon_{max}$ ($M^{-1}\ cm^{-1}$) are related by $f_{osc} = 4.61 \times 10^{-9}\epsilon_{max}\nu_{1/2}$.[92] Although both TD-DFT methods reproduce the key features in the experimental Abs spectrum reasonably well (after a uniform 4000 $cm^{-1}$ red-shift to account for the tendency of TD-DFT calculations to overestimate transition energies[44,71]), the most satisfactory agreement is obtained with the PW-LDA functional using models **Cbl-I** and **Cbi-I** (Figure 7).[93] Note that the TD-DFT/PW method properly predicts a small (175 $cm^{-1}$) blue-shift in the maximum of the Abs envelope in region ii upon replacement of the imidazole with a water, a prediction that is noticeably lacking in the TD-DFT/B3LYP-calculated Abs spectrum (cf., Figures 6 and S1).

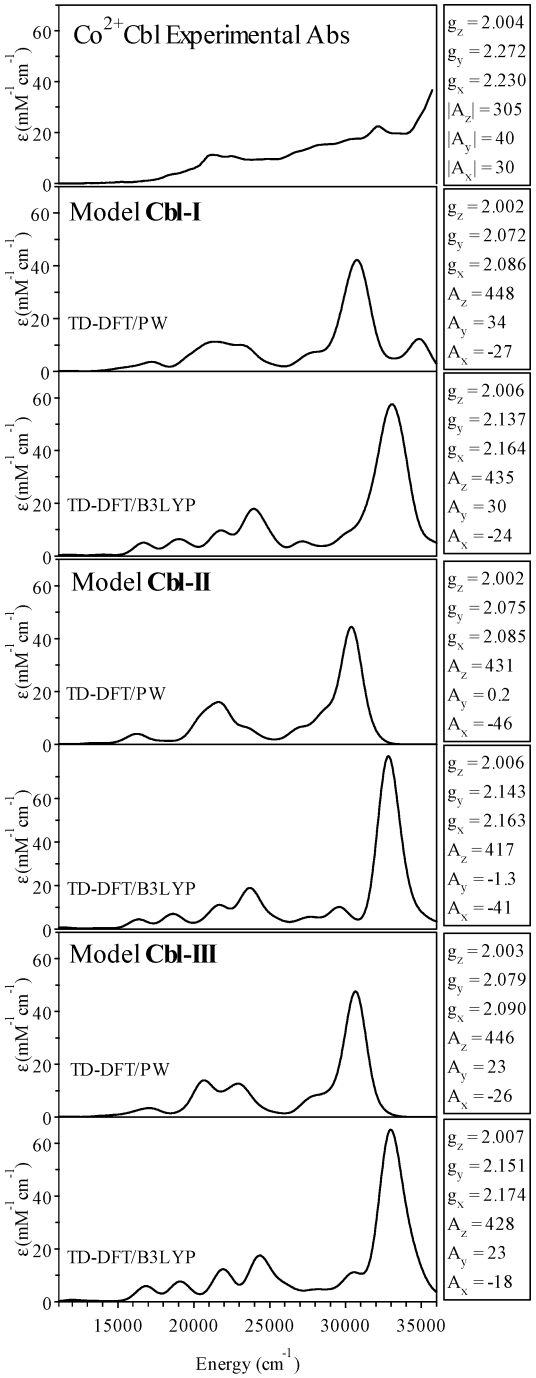


***Figure 6.*** Left: TD-DFT simulated Abs spectra for $Co^{2+}$Cbl using all combinations of geometries and functionals mentioned in the text. Right: Computed *g* values and $^{59}$Co hyperfine parameters (MHz). The experimental $Co^{2+}$Cbl Abs spectrum and EPR parameters[30] are given in the top panels.

DFT-computed EPR *g* values and cobalt hyperfine parameters for $Co^{2+}$Cbl models are listed on the right of Figure 6. While each calculation predicts EPR parameters that are in reasonable agreement with published data (Figure 6, top panel), the B3LYP hybrid functional consistently yields better agreement than the PW-LDA functional. Note that the computed EPR parameters are relatively insensitive to the choice of cofactor model, allowing us to focus entirely on models **Cbl-I** and **Cbi-I**. In the following, results from TD-DFT/PW calculations on **Cbl-I**

(91) Giorgetti, M.; Ascone, I.; Berrettoni, M.; Conti, P.; Zamponi, S.; Marassi, R. *J. Biol. Inorg. Chem.* **2000**, *5*, 156−166.
(92) Lever, A. B. P. *Inorganic Electronic Spectroscopy*, 2nd ed.; Elsevier: Amsterdam; New York, 1984.
(93) Similarly good agreement between PW and B3LYP TD-DFT-calculated Abs spectra was noted in our previous studies of various $Co^{3+}$corrinoids. In that case, the TD-DFT/B3LYP method was chosen to explore the natures of $Co^{3+}$corrinoid excited states because this method afforded a slightly better description of certain subtle features of the experimental Abs spectra (see ref 9 for details).

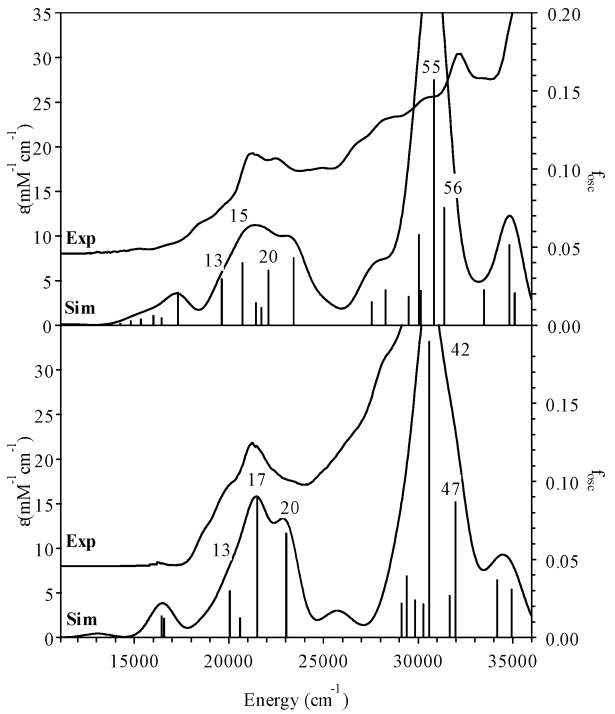


***Figure 7.*** TD-DFT/PW-calculated Abs spectra of $Co^{2+}$Cbl (top) and $Co^{2+}Cbi^{+}$ (bottom) along with experimental 4.5 K Abs data. Calculated spectra were red-shifted by 4000 cm$^{-1}$ to facilitate comparison with the experimental data. Transitions producing the dominant contributions to the computed Abs envelope are indicated by solid vertical lines.

and **Cbi-I** are therefore used to explore the excited-state properties of $Co^{2+}$corrinoids, whereas results obtained with the B3LYP hybrid functional are employed to examine the corresponding ground-state properties. The different choice of functional for calculating Abs spectra and EPR parameters is rationalized by the fact that while Abs spectroscopy probes the excited-state structure of the system, EPR spectroscopy intrinsically probes the ground-state wave function. Also note that both pure DFT and B3LYP calculations consistently led to at least qualitative agreement with all of the aforementioned experimental properties, and the same basic conclusions would thus be drawn regardless of the functional used. However, as the goal of this study is to perform a quantitative interpretation of the spectroscopic results obtained for $Co^{2+}$Cbl and $Co^{2+}Cbi^{+}$, the computational methods that afford the highest level of agreement between experiment and calculation are considered here.

**Ground-State Descriptions.** EPR spectroscopy has long been used to investigate the paramagnetic $Co^{2+}$ center and its interaction with the axial ligand in $Co^{2+}$corrinoids.[29−32] Recent advances in multidimensional pulsed EPR techniques also permitted measurement of hyperfine constants for the corrin ring nitrogens.[29,30] Together, $g$ values and hyperfine parameters provide an excellent basis for further evaluating our computed ground-state descriptions of $Co^{2+}$corrinoid species.

**(i) $Co^{2+}$Cbl.** Table 2 compares computed EPR $g$ value and $^{59}$Co ($I = {}^{7}/_{2}$) and $^{14}$N ($I = 1$) hyperfine constants obtained using the **Cbl-I** model (based on the crystal structure coordinates of $Co^{2+}$Cbl) to those determined experimentally. Our calculations properly predict the nearly axial **g**-tensor (2.272, 2.230, 2.004) and orientation of the in-plane components ($g_x$ and $g_y$) deduced by Harmer et al.,[30] which bisect the Co−N bond

***Table 2.*** Computed and Experimental EPR $g$ Values and Hyperfine Coupling Constants (MHz) for $Co^{2+}$Corrinoids[a]

| $Co^{2+}$Cbl | $g_x$ | $g_y$ | $g_z$ | $A_x$(Co) | $A_y$(Co) | $A_z$(Co) | $A_{iso}(N_{ax})$ |
|---|---|---|---|---|---|---|---|
| CP-SCF | 2.164 | 2.137 | 2.006 | −24 | 30 | 435 | 50 |
| exp[b] | 2.230 | 2.272 | 2.004 | 30 | 40 | 305 | 48 |
| $Co^{2+}Cbi^{+}$ | $g_x$ | $g_y$ | $g_z$ | $A_x$(Co) | $A_y$(Co) | $A_z$(Co) | |
| CP-SCF | 2.218 | 2.193 | 2.007 | 134 | 172 | 535 | |
| exp[c] | 2.320 | 2.320 | 1.997 | 213 | 213 | 395 | |

[a] Contributions to the calculated $^{59}$Co hyperfine tensor are detailed in Tables S9 and S10. [b] See ref 30. [c] See ref 29.

vectors.[94] While the axial component of the $^{59}$Co hyperfine tensor is considerably overestimated, the predicted in-plane values as well as the corrin ring $^{14}$N hyperfine values (2−5 MHz) are very close to the experimental values.

**(ii) $Co^{2+}Cbi^{+}$.** The B3LYP-calculated **g**-tensor as well as metal and ligand hyperfine parameters for this species are also in reasonable agreement with experimental data. The increase in calculated (and experimental) $g$ values relative to those of $Co^{2+}$Cbl reflects the expected decrease in Co $d_{z^2} \leftrightarrow d_{xz},d_{yz}$ energy splitting caused by stabilization of the occupied Co $d_{z^2}$-based MO following replacement of the strongly $\sigma$-donating DMB nitrogen with a weakly donating $H_2O$ molecule.[95] While the magnitude of the $z$-component of the computed $^{59}$Co hyperfine tensor is again overestimated, it is important to note that the increase in all hyperfine values from $Co^{2+}$Cbl to $Co^{2+}Cbi^{+}$ is nicely reproduced by our calculations. Examination of both Mulliken and Löwdin spin densities reveals that approximately 0.05 more spin resides on the metal center in $Co^{2+}Cbi^{+}$ than in $Co^{2+}$Cbl, providing a qualitative explanation for the observed increase in $^{59}$Co hyperfine values upon ligand substitution.

**Excited-State Descriptions. (i) $Co^{2+}$Cbl.** The TD-DFT-computed $Co^{2+}$Cbl Abs spectrum (Figure 7, top) reproduces all major features observed in the experimental spectrum remarkably well. The calculation predicts several electronic transitions of primarily cor $\pi \rightarrow \pi^*$ character centered in the visible region that almost quantitatively reproduce the Abs envelope in region ii of the experimental spectrum ($\lambda_{max}$ = 21 100 cm$^{-1}$/474 nm). To lower energy, several weak electronic transitions are predicted to occur, all of which possess significant $Co^{2+}$ d → d character, consistent with the large experimental $C/D$ ratios associated with bands 1−4 (Figure 3, bottom). The near UV region (region iii) of the calculated Abs spectrum is dominated by a single transition at 30 850 cm$^{-1}$ that is polarized along the Co···C$^{10}$ vector (short-axis) of the corrin ring. Transitions to nearby excited states are predicted to possess significant C$^5$···C$^{15}$ (i.e., perpendicular) polarization and substantial contributions from $Co^{2+}$ d-based orbitals; thus, spin−orbit mixing between these states and the excited state corresponding to the dominant short-axis polarized transition is likely

(94) Energies of $Co^{2+}$Cbl ligand field excited states were predicted using the first-order approximation for $g$ values of $S = {}^{1}/_{2}$ systems and the experimental $g$ shifts of 0.272 and 0.230 (see ref 30), yielding $\Delta E_{xz-z^2}$ = 11 360 cm$^{-1}$ and $\Delta E_{yz-z^2}$ = 13 435 cm$^{-1}$. These values are somewhat lower than the lowest-energy ligand field transitions observed in the MCD spectrum of $Co^{2+}$Cbl, implying that additional excited states contribute to the orbital angular momentum in the ground state via spin−orbit coupling.

(95) Deviations of $g_x$ and $g_y$ from $g_e = 2.00$ are due largely to the mixing of orbital angular momentum into the ground state associated with the matrix elements $\langle d_{z^2}|l_x|d_{yz}\rangle$ and $\langle d_{z^2}|l_y|d_{xz}\rangle$, respectively. As the energy separation between the ground state and the $d_{xz} \rightarrow d_{z^2}$ and $d_{yz} \rightarrow d_{z^2}$ excited states decreases, the $g$ shifts increase.

***Table 3.*** TD-DFT/PW-Calculated Energies (in $cm^{-1}$), Percent Contributions from Dominant One-Electron Excitations, and Oscillator Strengths for the Major Electronic Transitions of $Co^{2+}$Cbl

| state | $E$ ($cm^{-1}$) | f | transition | % | donor MO | acceptor MO |
|---|---|---|---|---|---|---|
| 2 | 10 090 | 0.0007 | 111b → 113b | 84 | Co $3d_{yz}$/cor-$\pi$ ($\beta$-HOMO) | Co $3d_{z^2}$ |
| 3 | 11 605 | 0.0005 | 111b → 112b | 53 | Co $3d_{yz}$/cor-$\pi$ ($\beta$-HOMO) | cor-$\pi$* ($\beta$-LUMO) |
| | | | 111a → 113a | 34 | Co $3d_{yz}$/cor-$\pi$ | cor-$\pi$* ($\alpha$-LUMO) |
| 5 | 14 250 | 0.0009 | 112a → 114a | 92 | Co $3d_{z^2}$ ($\alpha$-HOMO) | cor-$\pi$* |
| 6 | 14 810 | 0.0025 | 110b → 112b | 63 | Co $3d_{xz}$/cor-$\pi$ | cor-$\pi$* ($\beta$-LUMO) |
| 7 | 15 345 | 0.0037 | 109b → 112b | 49 | cor-$\pi$ | cor-$\pi$* ($\beta$-LUMO) |
| | | | 110a → 113a | 38 | cor-$\pi$ | cor-$\pi$* ($\alpha$-LUMO) |
| 8 | 16 000 | 0.0059 | 112a → 115a | 46 | Co $3d_{z^2}$ ($\alpha$-HOMO) | Co $3d_{xy}$ |
| 9 | 16 440 | 0.0045 | 109b → 113b | 52 | cor-$\pi$ | Co $3d_{z^2}$ |
| 15 | 20 705 | 0.0397 | 108b → 112b | 24 | Co $3d_{x^2-y^2}$ | cor-$\pi$* ($\beta$-LUMO) |
| | | | 110a → 113a | 19 | cor-$\pi$ | cor-$\pi$* ($\alpha$-LUMO) |
| | | | 111a → 114a | 16 | Co $3d_{yz}$/cor-$\pi$ | cor-$\pi$* |
| | | | 109b → 112b | 11 | cor-$\pi$ | cor-$\pi$* ($\beta$-LUMO) |
| 20 | 22 095 | 0.0350 | 111a → 114a | 27 | Co $3d_{yz}$/cor-$\pi$ | cor-$\pi$* |
| | | | 111b → 114b | 16 | Co $3d_{yz}$/cor-$\pi$ ($\beta$-HOMO) | cor-$\pi$* |
| 55 | 30 845 | 0.1569 | 110a → 116a | 12 | cor-$\pi$ | cor-$\pi$* |
| 56 | 31 375 | 0.0750 | 106a → 114a | 46 | Co 3d | cor-$\pi$* |
| | | | 109a → 116a | 11 | Co $3d_{xz}$ | cor-$\pi$* |

***Table 4.*** TD-DFT/PW-Calculated Energies (in $cm^{-1}$), Percent Contributions from Dominant One-Electron Excitations, and Oscillator Strengths for the Major Electronic Transitions of $Co^{2+}Cbi^{+}$

| state | $E$ ($cm^{-1}$) | f | transition | % | donor MO | acceptor MO |
|---|---|---|---|---|---|---|
| 1 | 7330 | 0.0002 | 98b → 99b | 92 | Co $3d_{yz}$/cor-$\pi$ ($\beta$-HOMO) | Co $3d_{z^2}$ ($\beta$-LUMO) |
| 2 | 8975 | 0.0001 | 96b → 99b | 86 | Co $3d_{xz}$ | Co $3d_{z^2}$ ($\beta$-LUMO) |
| 3 | 12 270 | 0.0006 | 98b → 100b | 56 | Co $3d_{yz}$/cor-$\pi$ ($\beta$-HOMO) | cor-$\pi$* |
| | | | 98a → 100a | 35 | Co $3d_{yz}$/cor-$\pi$ | cor-$\pi$* ($\alpha$-LUMO) |
| 4 | 13 115 | 0.0027 | 99a → 100a | 76 | Co $3d_{z^2}$/cor-$\pi$ ($\alpha$-HOMO) | cor-$\pi$* ($\alpha$-LUMO) |
| 5 | 13 535 | 0.0009 | 97b → 99b | 84 | cor-$\pi$ | Co $3d_{z^2}$ ($\beta$-LUMO) |
| 6 | 15 980 | 0.0013 | 96b → 100b | 80 | Co $3d_{xz}$ | cor-$\pi$* |
| 17 | 21 495 | 0.0889 | 95b → 100b | 29 | Co $3d_{x^2-y^2}$ | cor-$\pi$* |
| | | | 97a → 100a | 24 | cor-$\pi$ | cor-$\pi$* ($\alpha$-LUMO) |
| | | | 97b → 100b | 15 | cor-$\pi$ | cor-$\pi$* |
| | | | 99a → 102a | 11 | Co $3d_{z^2}$/cor-$\pi$ ($\alpha$-HOMO) | Co $3d_{xy}$ |
| 20 | 23 030 | 0.0667 | 98a → 101a | 26 | Co $3d_{yz}$/cor-$\pi$ | cor-$\pi$* |
| | | | 99a → 102a | 18 | Co $3d_{z^2}$/cor-$\pi$ ($\alpha$-HOMO) | Co $3d_{xy}$ |
| | | | 98b → 101b | 14 | Co $3d_{yz}$/cor-$\pi$ ($\beta$-HOMO) | cor-$\pi$* |
| 42 | 30 580 | 0.1892 | 91b → 99b | 10 | cor-$\pi$ | Co $3d_{z^2}$ ($\beta$-LUMO) |
| 47 | 31 980 | 0.0867 | 96a → 103a | 37 | Co $3d_{xz}$ | cor-$\pi$* |
| | | | 94a → 101a | 14 | Co 3d | cor-$\pi$* |

responsible for the appearance of the intense pseudo *A*-term observed in region iii of the $Co^{2+}$Cbl MCD spectrum (Figure 3, center).

**(ii) $Co^{2+}Cbi^{+}$.** The TD-DFT-computed Abs spectrum for $Co^{2+}Cbi^{+}$ predicts all major features observed in the experimental spectrum (Figure 7, bottom; Table 4), including a group of cor $\pi \rightarrow \pi^*$ transitions in the visible region that are responsible for the broad Abs envelope in region ii and several $Co^{2+}$ d → d transitions at lower energy. TD-DFT calculations also predict an intense, short-axis polarized transition centered at 30 580 $cm^{-1}$ that correlates nicely to the peak observed in the low-temperature Abs spectrum (Figure 4, top). Spin−orbit mixing with nearby excited states that possess differently oriented transition moments may give rise to the pseudo *A*-term that dominates region iii of the MCD spectrum. Most importantly, our calculations properly predict both the large blue-shift of d → d transitions in region i and the subtle shifts of features in regions ii and iii of the experimental Abs spectra upon lower ligand substitution from $Co^{2+}$Cbl to $Co^{2+}Cbi^{+}$.

**3.3. Spectral Assignments.** Given the good agreement between TD-DFT-computed and experimental Abs spectra for $Co^{2+}$Cbl and $Co^{2+}Cbi^{+}$, it is reasonable to assign key features of our excited-state spectroscopic data using the DFT-calculated MO descriptions. Isosurface plots of the MOs involved in these transitions are presented in Figure 8. As each electronic transition has contributions from multiple one-electron excitations involving several donor and acceptor MOs, it is most convenient to analyze key electronic transitions through examination of electron density difference maps (EDDMs) that illustrate the change in the total electron density upon excitation (Figure 8, bottom).

**(i) $Co^{2+}$Cbl.** The lowest-energy features of the experimental spectra (bands 1−4 in region i, Figure 3) are assigned to transitions possessing primarily $Co^{2+}$ d → d character, as they

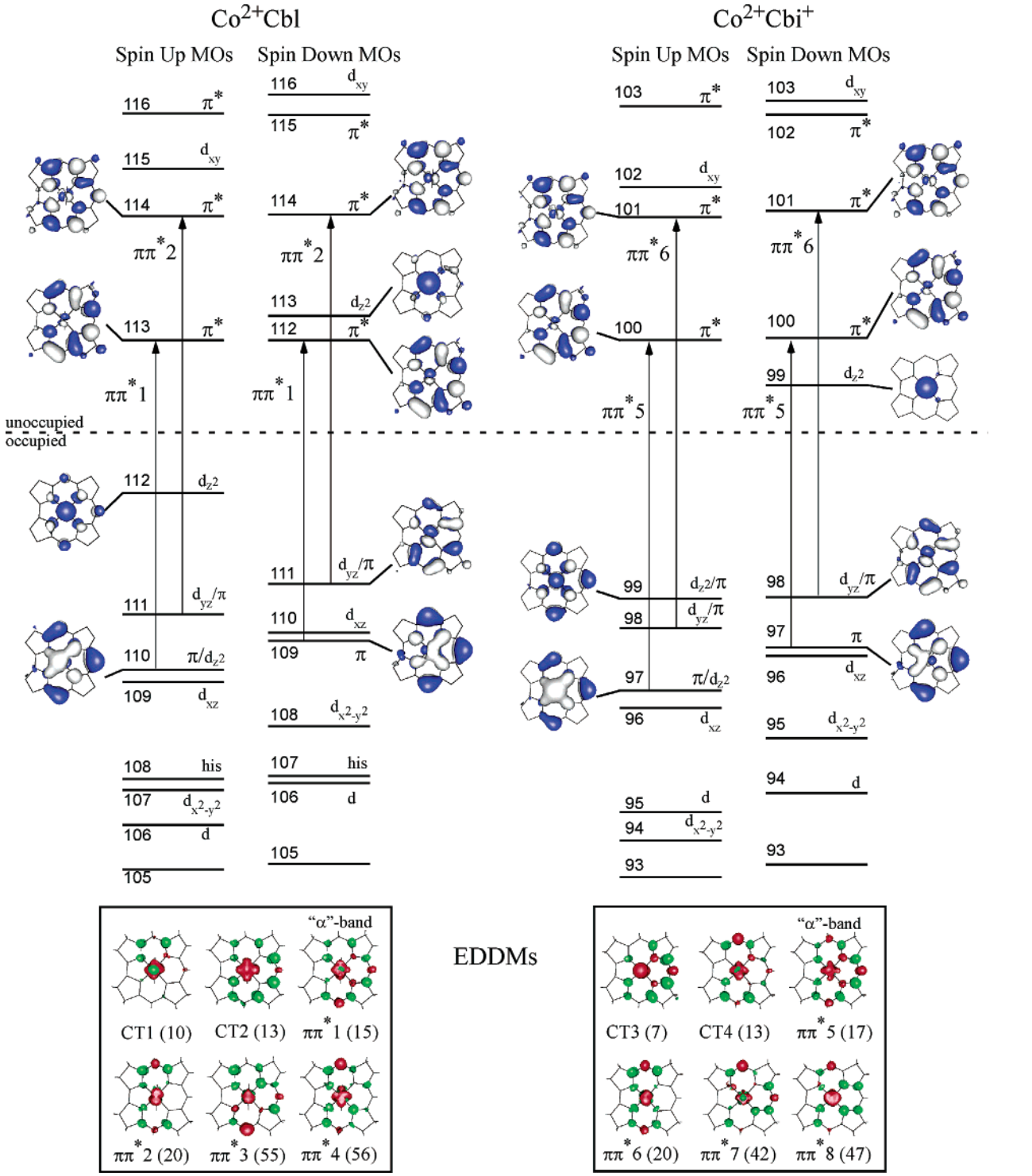


***Figure 8.*** Top: Isosurface plots of relevant MOs of $Co^{2+}$Cbl (left) and $Co^{2+}Cbi^{+}$ (right). MOs are designated by their dominant contributors and arranged according to their DFT-calculated energies (note that the HOMO/LUMO gap is not drawn to scale). The relevant electronic transitions contributing to the dominant bands in the TD-DFT-calculated spectra are indicated by arrows. Bottom: EDDMs for the transitions highlighted in the corresponding TD-DFT spectra (Figure 7). Red and green indicate loss and gain of electron density, respectively.

all exhibit large (≥0.03) *C*/*D* ratios. This finding is consistent with our TD-DFT calculations for $Co^{2+}$Cbl, which predict at least six electronic transitions mainly involving the $Co^{2+}$ 3d-based MOs, the first of which terminates in an MO with predominant $3d_{z^2}$ orbital character (state 2, Table 3).[96,97]

Examination of the EDDMs reveals that the lower energy transitions in region ii correspond to charge-transfer excitations from Co 3d- to corrin $\pi^*$-based MOs (EDDM CT1 and EDDM CT2, Figure 8) with intensities that are comparable to those of bands 5−7 in the experimental Abs spectrum. The higher energy

(96) TD-DFT/PW calculations underestimate charge transfer (CT) transition energies for states where vanishingly small orbital overlap exists between the donor and acceptor MOs (e.g., see state 1 of $Co^{2+}$Cbl, Table S7). It has recently been determined that this deficiency originates from the lack of Hartree−Fock exchange in TD-DFT/PW computations (see ref 97). Such states are ignored in our analysis, as their true transition energies would be much higher.

bands are dominated by an intense feature (band 8 centered at 21 100 $cm^{-1}$) that arises from a transition primarily cor $\pi \rightarrow \pi^*$ in character based on the preferential enhancement of corrin ring stretching modes in RR spectra obtained for laser excitation in this region (Figure 5). In support of this assignment, our TD-DFT computation predicts an intense long-axis polarized transition at 20 700 $cm^{-1}$ (state 15) whose EDDM is very similar in nature to that associated with the α-band of $Co^{3+}$corrinoids (vide infra) that corresponds to the lowest-energy cor $\pi \rightarrow \pi^*$ transition of those species.

On the basis of our computations, the most intense feature in region iii of the experimental Abs spectrum (band 18 at 32 470 $cm^{-1}$) is assigned as a short-axis polarized transition (state 55 at 30 850 $cm^{-1}$) involving significant cor $\pi \rightarrow \pi^*$ character, thus accounting for the large Abs intensity.

**(ii) $Co^{2+}$Cbi$^+$.** On the basis of our TD-DFT results, key transitions in the $Co^{2+}$Cbi$^+$ Abs spectrum can be classified similarly to those dominating the $Co^{2+}$Cbl Abs spectrum, as required by the close resemblance of the experimental Abs spectra for these two species. A cluster of $Co^{2+}$ d → d transitions is predicted to occur at low energy, consistent with the large *C*/*D* ratios observed for transitions contributing to region i of the Abs spectrum. Toward higher energy, these features are accompanied by a series of $Co^{2+}$ 3d → cor $\pi^*$ charge-transfer bands (e.g., state 13, EDDM CT4) that lead into the most intense region of the visible part of the Abs spectrum (region ii). The central feature at 21 275 $cm^{-1}$ (band 6, Figure 4) is identified as the lowest-energy cor $\pi \rightarrow \pi^*$ transition on the basis of our TD-DFT calculations, which predict an intense transition (state 17, EDDM $\pi\pi^*5$) that is similar in nature to the "α-transition" described above for $Co^{2+}$Cbl. The final feature of note is the well-resolved peak in the near UV region of the $Co^{2+}$Cbi$^+$ Abs spectrum (band 16) for which the TD-DFT calculation predicts a short-axis polarized transition moment (state 42, Table 4).

Comparison between the two sets of $Co^{2+}$corrinoid electronic spectra presented above indicates that lower ligand substitution has a profound effect on some transitions while only slightly perturbing others. The lowest-energy ligand field transition ($Co^{2+}$ $3d_{yz} \rightarrow 3d_{z^2}$) predicted for $Co^{2+}$Cbl (state 2, Table 3) is red-shifted by ~2760 $cm^{-1}$ in the computed $Co^{2+}$Cbi$^+$ Abs spectrum (state 1, Table 4) due to stabilization of the Co $3d_{z^2}$-based MO (MOs #112a and #99a, respectively; Figure 8) through relief of the Co-lower ligand σ-antibonding interaction upon DMB → $H_2O$ ligand exchange. Closer examination of the transition tables for these species (Tables 3 and 4) reveals an apparent interleaving of low energy transitions, whereby lower ligand substitution has the effect of blue-shifting transitions originating from MOs possessing significant Co $3d_{z^2}$ character (e.g., compare $Co^{2+}$Cbl state 8 and $Co^{2+}$Cbi$^+$ state 17) while red-shifting those terminating in MOs possessing significant Co $3d_{z^2}$ orbital character (as in the above example). This model accounts for the great differences observed in region i of the MCD spectra of $Co^{2+}$Cbl and $Co^{2+}$Cbi$^+$ (cf., Figures 3 and 4, center) but precludes establishment of a direct correlation between the first few transitions in these two data sets. The cor $\pi \rightarrow \pi^*$-based "α-transitions" are less affected by ligand substitution, as only a small blue-shift for this transition is observed experimentally (175 $cm^{-1}$) and predicted by our calculations (790 $cm^{-1}$). The electronic origin of this blue-shift is similar to that described above for the $Co^{2+}$ d → d-based transitions; however, the effect is much smaller in this case, as the donor MOs are cor $\pi^*$-based and thus possess little Co $3d_{z^2}$ orbital character and essentially no orbital contributions from the lower ligand. Last, the enormous derivative-shaped MCD feature in region iii is virtually invariant between $Co^{2+}$corrinoid species. Examination of the corresponding EDDMs ($\pi\pi^*3$ for $Co^{2+}$Cbl and $\pi\pi^*7$ for $Co^{2+}$Cbi$^+$; Figure 8) reveals that while each transition involves significant Co 3d orbital character (consistent with the large *C*/*D* ratio), the electron density on the lower ligand remains essentially constant. Collectively, these findings imply that cor $\pi \rightarrow \pi^*$ transitions of $Co^{2+}$corrinoids are largely insulated from the perturbing effects of ligand substitution. This result provides a fascinating contrast to the marked sensitivity of cor $\pi \rightarrow \pi^*$ transitions of $Co^{3+}$corrinoids to axial ligand substitution. The origin of this striking difference and its implication with respect to enzymatic Co−C bond activation and modulation of the $Co^{2+/+}$ redox couple are discussed below.

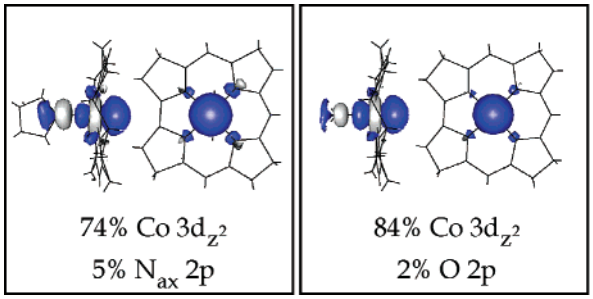


***Figure 9.*** Isosurface plots of the Co $3d_{z^2}$-based natural magnetic orbitals for $Co^{2+}$Cbl (left) and $Co^{2+}$Cbi$^+$ (right). The percent contributions from the Co $3d_{z^2}$ and axial ligand 2p atomic orbitals are indicated. In each case, the occupancy of the natural orbital is 1.000.

## 4. Discussion

EPR studies of $Co^{2+}$corrinoid species have played an integral role in probing the cofactor coordination in enzyme active sites since it was first discovered that a histidine residue could displace the intramolecular DMB ligand.[98] Although extremely sensitive to the nature of axial bonding in $Co^{2+}$corrinoids, EPR spectroscopy is essentially "blind" to the bulk of the cobalamin cofactor, most notably the corrin ring, as the single unpaired electron occupies the Co $3d_{z^2}$-based orbital that possesses little orbital contributions from the equatorial nitrogen atoms. This insulation of the unpaired electron from the macrocycle is particularly obvious upon examination of the isosurface plots of the singly occupied natural orbitals depicted in Figure 9,[99,100] which each show <3% total contribution from corrin ring nitrogens. Alternatively, due to the high intensity of cor $\pi \rightarrow \pi^*$ transitions, electronic Abs spectroscopy potentially offers an excellent probe of the geometric and electronic properties of the macrocycle. However, while numerous intense corrin-centered transitions are observed in all oxidation states of the cofactor, no attempts have been made to utilize these transitions as a reporter of corrin ring deformations in $Co^{2+}$corrinoids in any interpretive way. In this study, we have used multiple spectroscopic tools to obtain experimental insight into the

(97) Dreuw, A.; Head-Gordon, M. *J. Am. Chem. Soc.* **2004**, *126*, 4007−4016.
(98) Drennan, C. L.; Huang, S.; Drummond, J. T.; Matthews, R. G.; Ludwig, M. L. *Science* **1994**, *266*, 1669−1674.
(99) Green, M. T. *J. Am. Chem. Soc.* **1999**, *121*, 7939−7940.
(100) Green, M. T. *J. Am. Chem. Soc.* **2001**, *123*, 9218−9219.

electronic structures of $Co^{2+}$Cbl and $Co^{2+}$Cbi$^+$. Our Gaussian-resolved Abs and MCD spectra along with RR excitation profile data and previously published EPR parameters provided an excellent framework within which DFT electronic structure calculations could be evaluated. EPR parameters obtained using the CP-SCF method in conjunction with the hybrid B3LYP functional on cofactor models derived from published crystal structure coordinates of $Co^{2+}$Cbl yield reasonable agreement with EPR data and nicely reproduce the experimental trends in $g$ values and hyperfine parameters between $Co^{2+}$Cbl and $Co^{2+}$Cbi$^+$, lending credence to our calculated ground-state descriptions. TD-DFT-calculated Abs spectra for these same models using the PW-LDA functional closely match our experimental spectra (Figure 7), validating our computed excited-state descriptions.[101] Together, our combined spectroscopic/computational studies provide significant new insights into the electronic properties of $Co^{2+}$corrinoids. Key findings from these studies are summarized below, and their implications with respect to possible mechanisms of enzymatic modulation of the $Co^{2+/+}$ redox couple and stabilization of the $Co^{2+}$Cbl post-homolysis product are discussed.

**Axial Ligand Effects on $Co^{2+}$Corrinoid EPR Parameters.** Experimentally, replacement of the axial DMB base of $Co^{2+}$Cbl with a water molecule to generate $Co^{2+}$Cbi$^+$ increases the $A_z$ element of the $^{59}$Co hyperfine tensor by 95 MHz (Table 2).[29,30] Our calculations confirm the presiding belief that the change in $A_z$(Co) is due to a decrease in the covalent character of the $Co^{2+}-$lower ligand bond, as evidenced by a decrease in calculated bond order from 0.36 for $Co^{2+}-N_{ax}$ to 0.23 for $Co^{2+}-OH_2$ coincident with a 5% increase in spin density on the metal center. Interestingly, both experimental and computational data show that this change in axial ligation has a negligible effect on corrin ring $^{14}$N hyperfine values, which can be understood in terms of the insignificant differences in DFT-calculated $Co-N_{eq}$ bond orders and corrin ring N spin densities for the two $Co^{2+}$corrinoid species investigated. The natural orbital isosurface plots in Figure 9 indicate that the Co $3d_{z^2}$-based MO carrying the single unpaired electron is almost perfectly oriented along the lower axial ligand bond, which minimizes its interaction with the corrin $\pi$ system. This finding suggests that changes in corrin conformation will not markedly influence $Co^{2+}$corrinoid EPR parameters. Consistent with this hypothesis, our computations on $Co^{2+}$Cbl models that differ with respect to corrin ring fold angle afford nearly identical EPR parameters (cf., **Cbl-I**, **Cbl-II**, and **Cbl-III**; Figure 6). Considering all of this evidence collectively, it is apparent that EPR spectroscopy alone is poorly suited to study possible enzymatic Co−C bond activation schemes involving corrin ring deformations.

**Axial Ligand Effects on $Co^{2+}$Corrinoid Electronic Spectra.** Our TD-DFT-assisted spectral analysis reveals that the central feature in region ii of the $Co^{2+}$Cbl Abs spectrum (band 8, Figure 3) is attributable to the lowest-energy corrin-centered $\pi \rightarrow \pi^*$ transition originating from the HOMO-2 (MO #110a; Figure 9, left). As the primary acceptor orbital (MO #113a) for this transition exhibits an alternating pattern of C=C $\pi$-bonding and $\pi^*$-antibonding interactions quite different from that displayed by the donor MO, a considerable deformation of the corrin $\pi$-bonding network would be expected to occur in the corresponding excited state, consistent with preferential enhancement of corrin-based vibrations in RR spectra obtained for excitation in region ii. Interestingly, the pair of donor and acceptor MOs (Figure 9) for this transition is very similar in nature to that responsible for the prominent α-band in the Abs spectra of $Co^{3+}$corrinoids (vide infra). This $Co^{2+}$corrinoid "α-band" is blue-shifted by 175 cm$^{-1}$ in the $Co^{2+}$Cbi$^+$ Abs spectrum (band 6, Figure 4), as the primary donor orbital (MO #110a of $Co^{2+}$Cbl and #97a of $Co^{2+}$Cbi$^+$, Figure 8), while mostly corrin $\pi$ in character, also contains a small contribution from the Co $3d_{z^2}$ orbital that is $\sigma$-antibonding with respect to the lower axial ligand. As this antibonding interaction is mitigated upon replacement of the DMB with a weak water donor, all transitions originating from $Co^{2+}$Cbl MO #110a are slightly blue-shifted in the Abs spectrum of $Co^{2+}$Cbi$^+$ (where this donor orbital corresponds to MO #97a).

Several $Co^{2+}$ d $\rightarrow$ d transitions are unambiguously identified here for the first time in region i of the electronic spectra of both $Co^{2+}$corrinoids studied. In comparison to the "α-band" described above (region ii), these transitions are considerably more perturbed by axial ligand substitution, with several bands shifting in energy from $Co^{2+}$Cbl to $Co^{2+}$Cbi$^+$. Most notably, stabilization of the Co $3d_{z^2}$-based MO results in a predicted 2760 cm$^{-1}$ red-shift of the lowest-energy transition terminating in this orbital (cf., state 2, Table 3 and state 1, Table 4). This increased sensitivity to the nature of the lower ligand can be attributed to the larger $\sigma$-antibonding character present in the Co $3d_{z^2}$-based LUMO relative to the HOMO-2. As the Co $3d_{z^2}$-based MO is the redox active orbital for cofactor reduction to $Co^+$, the predicted stabilization of this MO alludes to a mechanism whereby enzyme systems may tune the $Co^{2+/+}$ reduction potential by manipulation of the lower ligand.

The only well-resolved feature in region iii of the Abs spectrum of each $Co^{2+}$corrinoid (band 18 for $Co^{2+}$Cbl and band 16 for $Co^{2+}$Cbi$^+$; Figures 3 and 4, respectively) is attributed to a short-axis polarized cor $\pi \rightarrow \pi^*$ transition. Similar to the "α-band" described above, this transition is virtually unperturbed by substitution of the axial ligand based on its minor red-shift (550 cm$^{-1}$) in going from $Co^{2+}$Cbl to $Co^{2+}$Cbi$^+$. While multiple donor/acceptor pairs of MOs are involved in this transition, examination of the corresponding EDDMs (EDDMs $\pi\pi^*3$ and $\pi\pi^*7$; Figure 8) reveals that this excitation gives rise to negligible changes in the Co-lower ligand bonding interaction, offering a rationale for the insensitivity of this transition to the nature of the lower ligand.

**Correlation between $Co^{2+}$Corrinoids and Alkyl-$Co^{3+}$Corrinoids.** A qualitative comparison of Abs spectra of alkyl-$Co^{3+}$corrinoids (e.g., MeCbl and MeCbi$^+$) and $Co^{2+}$corrinoids (Figure 10A) offers two very intriguing findings. First, replacement of the DMB with a water molecule in the lower axial position has a striking effect on the appearance of the Abs spectra of alkyl-$Co^{3+}$corrinoids, whereas $Co^{2+}$corrinoid Abs spectra are virtually unaffected by this lower ligand substitution (vide supra). Second, a remarkable similarity exists between the Abs spectra of MeCbi$^+$ and $Co^{2+}$corrinoids, implying that Co-center reduction of alkyl-$Co^{3+}$Cbis and the

(101) Note that the best agreement is achieved upon application of a uniform red-shift of 4000 cm$^{-1}$ to the calculated spectra. A larger shift of 5500 cm$^{-1}$ was applied in our studies of $Co^{3+}$corrinoids (see ref 9) because the TD-DFT/B3LYP method consistently predicts higher excitation energies than the TD-DFT/PW method.

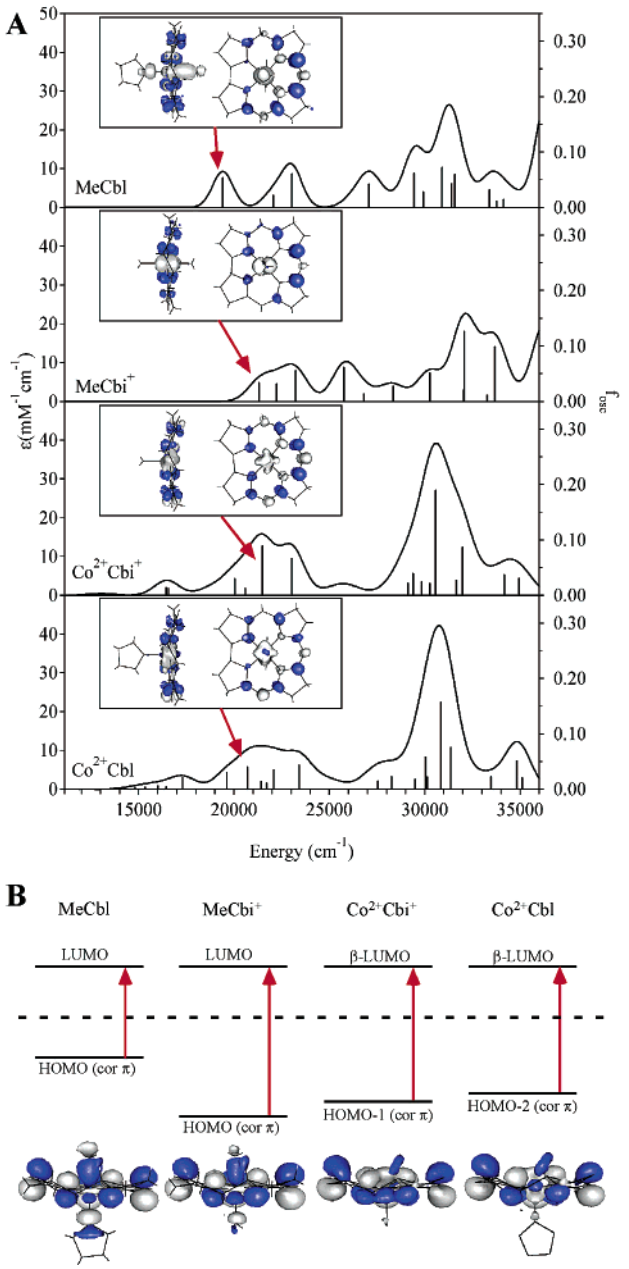


***Figure 10.*** (A) TD-DFT/PW simulated Abs spectra for (from top to bottom) MeCbl, $MeCbi^+$, $Co^{2+}Cbi^+$, and $Co^{2+}Cbl$. EDDMs are shown for the respective α-transitions. (B) Qualitative MO correlation diagram depicting (from left to right) the evolution of the MeCbl HOMO and LUMO upon lower ligand substitution to generate $MeCbi^+$, subsequent conversion to $Co^{2+}Cbi^+$, and, finally, lower ligand substitution to yield $Co^{2+}Cbl$. Red arrows indicate the α-transitions for each species. Isosurface plots of the corresponding donor MOs are shown at the bottom.

consequent upper axial ligand dissociation have surprisingly little effects on the corrin ring electronic structure.

Corrin-centered $\pi \rightarrow \pi^*$ transitions have long been assumed to dominate the Abs spectra of all $Co^{3+}$corrinoids, yet only recently has the effect of the axial ligands on these transitions been understood at an electronic level. As presented in our recent $Co^{3+}$corrinoid paper,[9] the extent of charge donation from the upper axial ligand to the metal center modulates the energy of the α-band, which corresponds to the lowest-energy cor $\pi \rightarrow \pi^*$ (HOMO → LUMO) transition. For example, the α-band red-shifts by ~1000 $cm^{-1}$ from $H_2OCbl^+$ to MeCbl, as the more strongly $\sigma$-donating methyl group gives rise to partial occupation of the $Co^{3+}$ $3d_{z^2}$ orbital, thereby inducing a large $Co-N_{ax}$ $\sigma$-antibonding interaction that destabilizes the HOMO (Figure 10, bottom). This $\sigma$-antibonding interaction is almost completely lost when the DMB lower ligand is replaced with a water molecule to generate $MeCbi^+$, which, therefore, leads to a substantial stabilization of the donor MO and consequently a blue-shift of the α-band by ~2500 $cm^{-1}$.

As noted above, $Co^{2+}$corrinoids also exhibit what we have classified as an "α-band" transition based on the similar nature of the corresponding donor/acceptor MOs (Figure 8) and EDDMs (Figure 10A) to those associated with the α-band of $Co^{3+}$corrinoids. Interestingly, our experimental data reveal that this α-band in $Co^{2+}$corrinoids blue-shifts by a mere 175 $cm^{-1}$ upon displacement of the DMB ligand of $Co^{2+}Cbl$ by a water molecule in $Co^{2+}Cbi^+$. This result can be understood by inspection of the isosurface plots of the MOs involved in this transition, which indicate that in each case the donor orbital (Figure 10B) has negligible contributions from the lower axial ligand and, therefore, is largely unperturbed upon axial ligand substitution.

The high degree of similarity between the Abs spectra of $MeCbi^+$ and $Co^{2+}Cbi^+$, especially in the region of the α-band (region ii, Figure 10), is quite unexpected given the change in coordination number and formal reduction of the $Co^{3+}$ center accompanying the conversion of $MeCbi^+$ to $Co^{2+}Cbi^+$. However, our DFT calculations reveal that the actual charge of the Co center is very similar in both $MeCbi^+$ and $Co^{2+}Cbi^+$, suggesting that the strongly donating methyl group imparts significant $Co^{2+}$ character onto the $Co^{3+}$ metal center and thus causes a similar perturbation of the α-band via the charge donation mechanism described above. Yet MeCbl, which also has considerable $Co^{2+}$ character induced by the methyl group, exhibits what is termed a "unique" Abs spectrum that is strikingly different from those of $MeCbi^+$ and the two $Co^{2+}$corrinoid species studied here (Figure 10A), exhibiting the α-band at substantially lower energy. Examination of the α-transition EDDMs for each species reveals that the HOMO → LUMO excitation for MeCbl is unique in that it also causes significant loss of electron density centered on the axial ligands. This finding provides evidence for a mechanism of excited-state stabilization mediated by simultaneous electron donation from both axial ligands, rationalizing the much lower α-transition energy for MeCbl. As this mechanism is exclusive to MeCbl, we propose that the "unique" Abs spectrum of this species results from the extensive $\sigma$-donation from the alkyl ligand, which leads to partial population of the Co $3d_{z^2}$ orbital and thus induces a strong $Co-N_{ax}$ $\sigma$-antibonding interaction with the trans DMB ligand. Because substitution of the DMB by a water molecule in the lower axial position almost completely eliminates this induced $\sigma$-antibonding interaction, $MeCbi^+$, $Co^{2+}Cbi^+$, and $Co^{2+}Cbl$ have similar excited-state electronic structures and hence they exhibit similar Abs spectra.

**Implications with Respect to Enzymatic Co−C Bond Activation Mechanisms.** An enduring topic of intense AdoCbl research is to develop an understanding of the $10^{12}$-fold rate enhancement for Co−C bond homolysis of the enzyme-bound cofactor.[4−7] Theories that attempt to rationalize this activation propose enzyme-induced destabilization of the $Co^{3+}Cbl$ "ground state", stabilization of the $Co^{2+}Cbl$/Ado• post-homolysis products, or a combination thereof. Using MMCM as an archetypal

example, RR studies by Spiro, Banerjee, and co-workers have shown that the Co−C bond weakens by a mere 0.5 kcal/mol upon binding of AdoCbl to the enzyme active site.[13,102−104] Recent experimental and computational results from our group confirmed this finding, as the minor observed shifts of the α-band upon cofactor binding to MMCM could be quantitatively correlated to negligibly small distortions of the cofactor's organometallic bond in the $Co^{3+}$ ground state.[10] Therefore, all current experimental evidence hints toward a mechanism of enzymatic Co−C bond activation involving stabilization of the $Co^{2+}$Cbl/Ado• post-homolysis products.

As shown above, our DFT calculations predict that the Co centers of MeCbl (and, by analogy, AdoCbl) and $Co^{2+}$Cbl possess remarkably similar charges. This result can be understood in terms of the extensive charge donation from the axial alkyl group to the cobalt center in AdoCbl, thereby imposing considerable $Co^{2+}$ character on the Co−C bond homolysis "precursor". This similarity in metal charge may reduce the reorganization energy associated with Co−C bond cleavage and the subsequent recombination of the homolysis products. Hence, to increase the rate constant for Co−C bond homolysis, the enzyme could manipulate the covalency of the $Co^{2+}$−lower ligand bond to even better match the charge at the Co center in AdoCbl. While in the case of $Co^{3+}$corrinoids, enzymatic manipulation of the axial bonding interactions can be conveniently probed by the α-band position, our $Co^{2+}$corrinoids studies presented here show that the α-band is no longer sensitive to the nature of the lower ligand, as the corresponding donor and acceptor MOs contain negligible axial ligand orbital character (Figure 10B). Conversely, the energies of the $Co^{2+}$ d → d transitions that dominate region i of the $Co^{2+}$corrinoid MCD spectra are clearly attuned to the nature of the lower ligand and may thus serve as excellent reporters of enzyme-induced perturbation of axial bonding interactions. Indeed, our preliminary MCD data obtained for MMCM-bound $Co^{2+}$Cbl show significant changes in the energies of these transitions, which become even more pronounced in the presence of substrate analogues. Quantitative analysis of these spectral changes within the theoretical framework developed in this study will provide significant new insight into enzymatic stabilization of the $Co^{3+}$Cbl post-homolysis products and, thus, the mechanism of Co−C bond activation.

In stark contrast to AdoCbl-dependent systems, MeCbl-dependent enzymes proceed directly to four-coordinate $Co^{+}$Cbl via heterolysis of the Co−C bond, which effectively populates the Co $3d_{z^2}$ orbital with two electrons. A fascinating aspect of these enzymes is that they must accommodate the two electrons to form the $Co^{+}$Cbl state while simultaneously preventing the detrimental formation of $Co^{2+}$Cbl. This remarkable selectivity may be achieved through modulation of the Co $3d_{z^2}$ orbital energy, for example, by weakening, or even eliminating, the bonding interaction with the lower ligand. However, direct experimental observation of such enzyme-induced destabilization of $Co^{2+}$Cbl in favor of the desired $Co^{+}$Cbl state has yet to be achieved. As shown in this study, alteration of the $Co^{2+}$ 3d orbital energies through changes in the axial ligand set elicits striking changes in region i of the MCD spectra of $Co^{2+}$corrinoids. Indeed, our preliminary investigations of $Co^{2+}Cbi^{+}$ bound to the $Co^{+}$corrinoid:ATP adenosyltransferase (CobA) in the presence of the cosubstrate ATP (Figure 11) yield MCD spectra unlike any of those presented above, suggesting a significant change in the $Co^{2+}$ coordination environment upon cofactor binding to the protein active site. CobA has been shown to adenosylate a wide range of cobalamin precursors, including $Co^{2+}Cbi^{+}$,[25,27] where in each case the corrinoid substrate is first reduced to the $Co^{+}$ oxidation state by a flavoprotein (FldA) prior to adenosyl group transfer from ATP.[28,45] As $Co^{+}$corrinoids possess a four-coordinate Co center that is solely ligated by the corrin ring, we have explored the effect of a systematic lengthening of the $Co-OH_2$ bond toward this four-coordinate limit on the Abs spectrum of $Co^{2+}Cbi^{+}$ using TD-DFT computations. These calculations indicate that as the water ligand is removed, the $Co^{2+}$ $3d_{yz} \rightarrow 3d_{z^2}$ transition drops in energy, consistent with the observed perturbation of features in region i of the MCD spectrum upon $Co^{2+}Cbi^{+}$ binding to CobA. While a quantitative analysis of these striking spectral changes is currently underway, we suggest that CobA-bound $Co^{2+}Cbi^{+}$ may be the first spectroscopically characterized example of a species with electronic properties consistent with a four-coordinate $Co^{2+}$corrinoid.

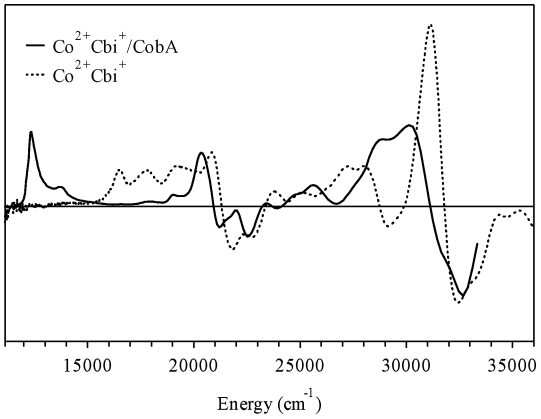


***Figure 11.*** 7 T 4.5 K MCD spectra of $Co^{2+}Cbi^{+}$ bound to CobA (solid line) as compared to free $Co^{2+}Cbi^{+}$ (dotted line).

**Acknowledgment.** We acknowledge Prof. Jorge Escalante-Semerena for useful discussions. T.C.B. thanks the University of Wisconsin, NSF (CAREER grant MCB-0238530), Sloan Research Foundation, and The Research Corporation (Award No. RI0596) for financial support and Dr. Frank Neese (MPI Mülheim) for supplying a free copy of the ORCA software package and for his continued advice regarding DFT computations. N.R.B. was supported by a Howard Hughes Medical Institute Predoctoral Fellowship and by NIH grant GM40313 to J. C. Escalante-Semerena.

**Supporting Information Available:** Cartesian coordinates for all computational models, TD-DFT results for those models and isosurface plots of the MOs for models discussed in the text, and variable-temperature MCD spectra for $Co^{2+}$Cbl. This information is available free of charge via the Internet at http://pubs.acs.org.

JA0481631

(102) Dong, S. L.; Padmakumar, R.; Banerjee, R.; Spiro, T. G. *J. Am. Chem. Soc.* **1996**, *118*, 9182−9183.
(103) Dong, S. L.; Padmakumar, R.; Banerjee, R.; Spiro, T. G. *J. Am. Chem. Soc.* **1999**, *121*, 7063−7070.
(104) Dong, S. L.; Padmakumar, R.; Maiti, N.; Banerjee, R.; Spiro, T. G. *J. Am. Chem. Soc.* **1998**, *120*, 9947−9948.